



CHALMERS
UNIVERSITY OF TECHNOLOGY

Avoiding decoherence with giant atoms in a two-dimensional structured environment




Downloaded from: <https://research.chalmers.se>, 2024-12-20 02:29 UTC

Citation for the original published paper (version of record):

Raaholt Ingelsten, E., Frisk Kockum, A., Soro Álvarez, A. (2024). Avoiding decoherence with giant atoms in a two-dimensional structured environment. *Physical Review Research*, 6(4).
<http://dx.doi.org/10.1103/PhysRevResearch.6.043222>

N.B. When citing this work, cite the original published paper.

Avoiding decoherence with giant atoms in a two-dimensional structured environment

Emil Raaholt Ingelsten , Anton Frisk Kockum , and Ariadna Soro *

Department of Microtechnology and Nanoscience, *Chalmers University of Technology*, 412 96 Gothenburg, Sweden



(Received 11 June 2024; accepted 16 October 2024; published 2 December 2024)

Giant atoms are quantum emitters that can couple to light at multiple discrete points. Such atoms have been shown to interact without decohering via a one-dimensional waveguide. Here, we study how giant atoms behave when coupled to a two-dimensional square lattice of coupled cavities, an environment characterized by a finite-energy band and band gaps. In particular, we describe the role that bound states in the continuum (BICs) play in how giant atoms avoid decoherence. By developing numerical methods, we are able to investigate the dynamics of the system and show the appearance of interfering BICs within a single giant atom, as well as oscillating BICs between many giant atoms. In this way, we find the geometric arrangements of atomic coupling points that yield protection from decoherence in the two-dimensional lattice. These results on engineering the interaction between light and matter may find applications in quantum simulation and quantum information processing.

DOI: [10.1103/PhysRevResearch.6.043222](https://doi.org/10.1103/PhysRevResearch.6.043222)

I. INTRODUCTION

In the past decade, a new paradigm of quantum emitters has been increasingly attracting interest: so-called giant atoms (GAs) [1]. These atoms, which may be artificial, earn their name by breaking the dipole approximation: the assumption that atoms are *small* compared to the wavelength of the field they interact with. *Giant* atoms instead couple to light (or other bosonic fields) at several discrete points, which can be spaced wavelengths apart. The interference between emission and absorption through these coupling points then leads to a plethora of remarkable features, such as frequency-dependent decay rates and Lamb shifts [2,3], waveguide-mediated decoherence-free interaction [4–9], and oscillating bound states [10–14].

Since 2014, several experimental demonstrations of GAs have been achieved, both with superconducting qubits coupled to surface acoustic waves [15–26] and to microwave waveguides [3,5,27], and several other implementations have been proposed [28,29]. Recently, giant-atom physics has also been explored beyond the atomic paradigm in giant molecules [30–34] or giant spin ensembles [35]. However, most studies to date (both theoretical and experimental) have focused on GAs coupled to one-dimensional reservoirs: most commonly to continuous waveguides [2–5,7,9–11,13,27,36–50], but recently also to structured ones [8,14,29,51–65].

Here, we instead study GAs coupled to a two-dimensional (2D) structured environment, modeled as a square lattice of coupled cavities with nearest-neighbor interaction (see Fig. 1).

This environment has been studied in depth in relation to small atoms [66–73], and there are additional works on small atoms coupled to other 2D [71,72,74–77] or higher-dimensional [70,78–80] structured environments. However, GAs in a 2D square lattice have only received limited attention so far: in Ref. [28], the focus was on engineering unconventional emission patterns from a single GA in a particular experimental implementation; in Ref. [72], the study revolved around harnessing topologically protected propagating modes; and in Ref. [81], the focus was on the analytical framework used to describe GAs coupled to photonic baths of any structure and dimension.

In this work, we describe the dynamics of GAs when they are tuned to the band of the 2D bath by developing numerical methods (split-operator approach) and using complex-analysis techniques (resolvent formalism). We specifically focus on ways the GAs can avoid decoherence. In doing so, we find that bound states in the continuum [82–85] (BICs) arise in certain geometries and make it possible for GAs to exhibit both subradiance and decoherence-free interaction. We also show different interference patterns of the BICs enclosed by eight coupling points of a single GA. Moreover, by studying the bound-state dynamics, we identify decoherence-free interaction [4,5] as a many-atom analog of previously reported oscillating BICs [10–14]. Finally, we explore many-GA configurations that exploit decoherence-free interactions for potential applications in quantum simulation and computing, such as chains with pairwise interactions, triads with all-to-all interaction, and grids with effective long-range interactions.

This article is structured as follows. In Sec. II, we present and discuss a Hamiltonian model for GAs coupled to a 2D square lattice of coupled cavities. In Sec. III, we develop an efficient numerical method to simulate the dynamics of this system. The results from the simulations are shown in Sec. IV, where we focus on ways in which GAs become protected from decoherence and delve into the characterization of BICs.

*Contact author: soro@chalmers.se

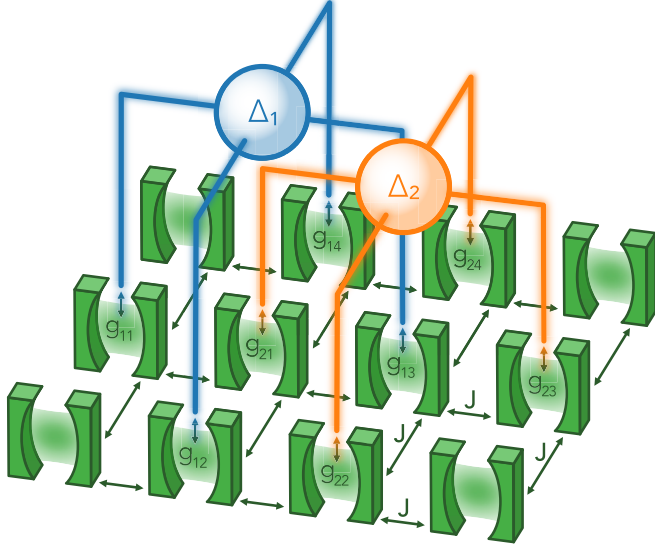


FIG. 1. Two giant atoms in a braided configuration coupled to a 2D structured bath. The bath is modeled as a square lattice of $N \times N$ cavities with resonance frequency ω_B and nearest-neighbor coupling strength J . The atoms are two-level systems, with transition frequencies ω_i detuned from the middle of the band by $\Delta_i = \omega_i - \omega_B$ ($i = 1, 2$). They are coupled to the cavities with coupling strength g_{ip} at each coupling point, where i refers to the atom and p to the connection point.

In particular, we investigate the subradiance of a single GA in Sec. IV A, the decoherence-free interaction between two GAs in Sec. IV B 1, and other configurations involving many GAs in Sec. IV B 2. We provide the code to reproduce all the results from Sec. IV in Ref. [86]. We conclude in Sec. V with a summary and an outlook. Moreover, we include Appendix A, where we show the resolvent-formalism techniques that support the results of this article, and Appendix B, where we provide additional details for the numerical method described in Sec. III. Finally, we also include Appendix C, where we describe how to engineer a perfectly subradiant GA detuned from the middle of the band, as well as setups exhibiting perfect subradiance at multiple different detunings, which has previously only been demonstrated in one-dimensional waveguides [5].

II. THEORETICAL FRAMEWORK

We start by deriving a Hamiltonian model for the setup shown in Fig. 1. Both the setup and the Hamiltonian are inspired by those presented in Refs. [8,28,66].

The structured 2D reservoir we consider can be described as a square lattice of $N \times N$ cavities with resonance frequencies ω_B and nearest-neighbor couplings J . Taking the separation of adjacent cavities as the unit of length, we characterize the position of each cavity with a coordinate vector $\vec{n} = (n_x, n_y)$, where $n_x, n_y \in [0, N - 1]$, and label each corresponding cavity annihilation operator as $a_{\vec{n}}$. The resulting bath Hamiltonian in real space, rotating at frequency ω_B , reads

($\hbar = 1$ throughout this article)

$$H_B = -J \sum_{\langle \vec{n}, \vec{m} \rangle} (a_{\vec{n}}^\dagger a_{\vec{m}} + \text{H.c.}), \quad (1)$$

where $\langle \vec{n}, \vec{m} \rangle$ denotes summation over all pairs of neighboring cavities at \vec{n} and \vec{m} , and H.c. denotes the Hermitian conjugate.

The Hamiltonian in Eq. (1) can be diagonalized by introducing periodic boundary conditions and the operators in momentum space

$$a_{\vec{n}} = \frac{1}{N} \sum_{\vec{k}} a_{\vec{k}} e^{-i\vec{k} \cdot \vec{n}}, \quad (2)$$

where $\vec{k} = (k_x, k_y)$ is the wave vector, with $k_x, k_y \in \{-\pi, \dots, \pi - \frac{2\pi}{N}\}$. In that basis,

$$H_B = \sum_{\vec{k}} \omega(\vec{k}) a_{\vec{k}}^\dagger a_{\vec{k}}, \quad (3)$$

with

$$\omega(\vec{k}) = -2J(\cos k_x + \cos k_y). \quad (4)$$

The dispersion relation in Eq. (4), although describing a fairly simple 2D structured bath, gives rise to some very interesting properties. First and foremost, it results in an energy band in the range $\omega(\vec{k}) \in [-4J, 4J]$. Within this band, the energy dispersion varies widely: it is isotropic close to the band edges, but becomes highly anisotropic at the band center [i.e., at $\omega(\vec{k}) = 0$] [66]. This is easy to see from the definition of group velocity: at $\omega(\vec{k}) = 0$,

$$\vec{v}_g = \vec{\nabla} \omega(\vec{k})|_{\omega(\vec{k})=0} = 2J \sin k \begin{bmatrix} 1 \\ \pm 1 \end{bmatrix} \quad (5)$$

for any $k \in \{-\pi, \dots, \pi - \frac{2\pi}{N}\}$. At the band center, excitations can thus only propagate along two orthogonal diagonals, which we hereafter refer to as the $\begin{bmatrix} 1 \\ \pm 1 \end{bmatrix}$ diagonals. Furthermore, note that \vec{v}_g vanishes for $k = \{0, \pm\pi\}$, which yields a divergent density of states, i.e., a type of Van Hove singularity present in many 2D structured baths [66,67].

We now consider M two-level GAs, with transition frequencies ω_i , detuned from the middle of the band by $\Delta_i = \omega_i - \omega_B$. The bare Hamiltonian of these GAs (rotating at ω_B) is

$$H_A = \sum_{i=1}^M \Delta_i \sigma_i^+ \sigma_i^-, \quad (6)$$

where σ_i^\pm denote the atomic ladder operators. If the i th GA couples to the bath at P_i points, then the interaction of the atoms with the bath under the rotating-wave approximation (RWA) can be described by

$$\begin{aligned} H_{\text{int}} &= \sum_{i=1}^M \sum_{p=1}^{P_i} g_{ip} (a_{\vec{n}_{ip}} \sigma_i^+ + \text{H.c.}) \\ &= \sum_{i=1}^M \sum_{p=1}^{P_i} \frac{g_{ip}}{N} \sum_{\vec{k}} (e^{-i\vec{k} \cdot \vec{n}_{ip}} a_{\vec{k}} \sigma_i^+ + \text{H.c.}), \end{aligned} \quad (7)$$

where \vec{n}_{ip} denotes the position of the cavity which interacts with the p th coupling point of the i th atom. The coupling strength between the atom and the bath at this point is g_{ip} , which we assume to be real for convenience. Although we leave complex coupling strengths out of the scope of this manuscript, we note that they are experimentally achievable [27,28,32,87] and can be used to engineer chiral emissions and interactions [27,28,32,35,43,47,87,88].

With the definitions above, the total Hamiltonian of the system is

$$H = H_B + H_A + H_{\text{int}}. \quad (8)$$

We note that this model is valid under the assumption of coupling to a single polarization of light and a single bosonic band. We focus on the single-excitation subspace for convenience, but the phenomena showcased throughout the paper still exist beyond this subspace. We also work in the continuum limit (i.e., $N \rightarrow \infty$ in the analytics, and $tJ \ll N/2$ in the simulations), which allows us to disregard effects arising from the finite size of the bath. Additionally, we neglect couplings to other reservoirs by assuming that the losses induced by such couplings occur at a significantly lower rate than the relevant dynamics we study. Last, we assume weak coupling strengths $g_{ip} < J$ and $g_{ip} \ll \omega_i, \omega_B \forall i, p$, to comply with the RWA we applied in Eq. (7).

This theoretical model may be used to describe cold atoms coupled to photonic crystals [69,89] or optical lattices [28,90,91], as well as superconducting qubits coupled to microwave photonic crystals [92–96] or superconducting metamaterials [97–103]. Due to the intricate nature of the setup (2D resonator lattice *and* multiplicity of atoms *and* multiplicity of coupling points per atom arranged in a non-trivial manner), the experimental realization of cold atoms in the GA regime requires excellent control of a dynamical state-dependent optical lattice [28]. Such an implementation remains elusive to date, and we thus consider our setup to be most readily implementable with superconducting qubits. We note that, in such a case, arranging for the multiple coupling points may be aided by flip-chip technology [104–106].

III. NUMERICAL METHODS

The aforementioned Van Hove singularities [see Sec. II, after Eq. (5)] in the middle of the band and at the band edges introduce branch cuts that make it hard to analytically calculate how the exact atomic and bath populations evolve over time. While we provide derivations for those quantities in Appendix A, we rely heavily on numerical simulations to study the dynamics of the system. In this section, we present the numerical methods we develop and use in this work.

We base our numerical method on a so-called *split-operator* approach [107], which has been used in previous studies of small and giant atoms coupled to structured environments [8,66]. Essentially, this method is based on splitting the full Hamiltonian in Eq. (8) into the bath part H_B [diagonal in Fourier space, Eq. (3)], the atomic part H_A [diagonal in real space, Eq. (6)], and the interaction part H_{int} [Eq. (7)], and evolving the system by repeatedly applying the approximate

time-evolution operator

$$\tilde{U}(\Delta t) = \mathcal{F}^{-1} U_B(\Delta t) \mathcal{F} U_A(\Delta t), \quad (9)$$

where

$$U_A(\Delta t) = e^{-i(H_A + H_{\text{int}})\Delta t}, \quad U_B(\Delta t) = e^{-iH_B\Delta t}, \quad (10)$$

and \mathcal{F} denotes a Fourier transform, implemented in practice as a fast Fourier transform (FFT). While this is not equivalent to applying the exact time-evolution operator $U(t) = \exp[-i(H_B + H_A + H_{\text{int}})t]$, it is accurate to $\mathcal{O}(\Delta t^3)$, provided that the copies of $\tilde{U}(\Delta t)$ are sandwiched between an initial $U_A(-\Delta t/2)$ and a final $U_A(\Delta t/2)$ [108].

Since U_B is diagonal in Fourier space, it is trivial to compute. The same does not hold for U_A in real space due to the presence of H_{int} . However, for small atoms, it has been previously used [66] that, as long as no cavity couples to multiple atoms, U_A can be calculated with a computational complexity linear in M and N^d , where d is the dimensionality of the bath (in our case: $d = 2$). The reason for this complexity can most easily be seen by examining the structure of $H_A + H_{\text{int}}$.

Defining the state vector for our system such that the first M elements correspond to the (bare) atomic excited states and the following N^2 elements correspond to the states where one of the cavities is excited (and the atoms are in their ground states), we can write the combined atomic and interaction Hamiltonian as a block matrix:

$$H_A + H_{\text{int}} = \begin{bmatrix} D & \Gamma \\ \Gamma^T & \mathbb{0} \end{bmatrix}. \quad (11)$$

Here, D is a diagonal $M \times M$ matrix containing the detunings Δ_i for the different atoms, Γ is an $M \times N^2$ matrix containing all terms related to atom-bath interaction, and $\mathbb{0}$ is the $N^2 \times N^2$ zero matrix. For the case of small atoms, where atom i couples to a single cavity with coupling strength g_i ,

$$[\Gamma]_{in} = \begin{cases} g_i & \text{if atom } i \text{ couples to cavity } n, \\ 0 & \text{otherwise.} \end{cases} \quad (12)$$

Assuming each cavity only couples to a single atom, no interaction occurs between atoms without taking H_B into account. Thus, each atom i is isolated and can be modeled using an effective Hamiltonian

$$H_i = \begin{bmatrix} \Delta_i & g_i \\ g_i & 0 \end{bmatrix}. \quad (13)$$

In other words, to apply U_A to a state, one only needs to evaluate M different 2×2 matrix exponentials:

$$U_i(\Delta t) = \exp(-iH_i\Delta t). \quad (14)$$

The matrix elements of U_i can then be used to apply the same time evolution as the one caused by U_A to atom i and its coupled cavity. This is significantly cheaper than computing U_A directly, which would entail computing an $(M + N^2) \times (M + N^2)$ matrix exponential. In turn, this would have a computational cost scaling like $(M + N^2)^3$, since the cost of exponentiating an $n \times n$ matrix in general scales like n^3 using state-of-the-art algorithms [109,110].

As described in Sec. II, the most general GA case involves each atom i coupling to P_i resonators with coupling strengths $\{g_{ip}\}_{p=1}^{P_i}$. As long as there are still no cavities coupling to multiple atoms, the small-atom method described above can

be generalized to handle GAs by simply extending the size of the effective Hamiltonian with an additional row and column for each added coupling point, such that

$$H_i = \begin{bmatrix} \Delta_i & \vec{g}_i \\ \vec{g}_i^T & \mathbb{0} \end{bmatrix}, \quad (15)$$

where \vec{g}_i is a $1 \times P_i$ row matrix with elements $[\vec{g}_i]_p = g_{ip}$. This Hamiltonian can then be used completely analogously to how H_i is used in the small-atom case.

However, as we show in Appendix B, we can generalize the small-atom method to handle GAs without increasing the size of the effective Hamiltonian. We can thus not only apply U_A to a state at a cost linear in M and N^2 for GAs, just as has previously been possible for small atoms, but the cost can be made linear in P_i . In contrast, the cost of exponentiating a $(1 + P_i) \times (1 + P_i)$ matrix directly would scale as $(1 + P_i)^3$. While this difference is not very significant for most of the configurations examined in this study, the P_i -linear version of the method would be significantly faster at modeling more complicated setups, e.g., ones based on reverse design like those described in Ref. [28]. Note that our generalized method works for baths of arbitrary dimensionality, but we focus mainly on the 2D case in this paper.

The P_i -linear method for computing the elements of U_A is based on using an effective Hamiltonian

$$H_i = \begin{bmatrix} \Delta_i & G_i \\ G_i & 0 \end{bmatrix}, \quad (16)$$

$$\left\{ \begin{array}{l} [\mathbb{1}_M + D_0]_{ij} = \delta_{ij}[U_i]_{11}, \\ [D_1\Gamma]_{in} = [\Gamma^T D_1]_{ni} = \begin{cases} \frac{g_{ipn}}{G_i}[U_i]_{12} & \text{if cavity } n \text{ couples to atom } i \text{ at point } p_n, \\ 0 & \text{otherwise,} \end{cases} \\ [\mathbb{1}_{N^d} + \Gamma^T D_2\Gamma]_{mn} = \begin{cases} \delta_{mn} + \frac{g_{ipm}g_{ipn}}{G_i^2}([U_i]_{22} - 1) & \text{if cavities } m, n \text{ couple to atom } i \text{ at } p_m, p_n, \\ \delta_{mn} & \text{otherwise.} \end{cases} \end{array} \right. \quad (20)$$

Applying the map encoded by U_A can thus be done, to accuracy $\mathcal{O}(\Delta t^3)$, with computational cost linear in M , N^2 , and P_i for GAs. Doing so moves the bottleneck of the split-operator algorithm to the computation of the time evolution associated with H_B . Specifically, the bottleneck becomes the two FFTs performed in each time step, which have complexity $\mathcal{O}(N^2 \log N)$ [111], since the computation and application of U_B in the bath eigenbasis only has complexity $\mathcal{O}(N^2)$.

As discussed in Ref. [66], the computational cost of the time-evolution algorithm can be reduced further by introducing an additional approximation based on going to the continuum limit, discretizing frequency space and exploiting the periodicity of $\omega(\vec{k})$.

IV. AVOIDING DECOHERENCE

In this section, we explore ways in which GAs can avoid relaxing into the bath. Therefore, we focus on the case $\Delta/J = 0$, where the atoms are tuned to the middle of the band and thus can only emit along two orthogonal diagonals, as shown in Sec. II [see the discussion around Eq. (5)]. This restriction in

where

$$G_i = \sqrt{\sum_{p=1}^{P_i} g_{ip}^2} \quad (17)$$

is the effective coupling strength of atom i . If the atom couples equally strongly to each coupling point, i.e., $g_{ip} = g_i$ for every p , then Eq. (17) reduces to

$$G_i = \sqrt{P_i}g_i. \quad (18)$$

Since the Γ block in Eq. (11) is now more complicated than in the small-atom case, the elements of U_A are more complicated than simply being copies of the elements in U_i when using our 2×2 effective Hamiltonian [Eq. (16)]. In fact, as shown in Appendix B, again assuming that no cavities couple to multiple atoms, U_A can be written as a block matrix

$$U_A = \begin{bmatrix} \mathbb{1}_M + D_0 & D_1\Gamma \\ \Gamma^T D_1 & \mathbb{1}_{N^2} + \Gamma^T D_2\Gamma \end{bmatrix}, \quad (19)$$

where $D_{0,1,2}$ are diagonal matrices that can be computed from the elements of U_i . Specifically, the matrix elements of $U_A(\Delta t)$ can be expressed as follows:

emission directions makes it relatively easy to engineer interference such that emission to the bath from different atoms, or from different coupling points belonging to the same atom, cancels completely [28,66–68,73]. For setups with $\Delta/J \neq 0$, see Appendix C.

A. Single giant atom—Subradiance

We typically refer to an ensemble of atoms that radiate to their environment at a slower rate than that given by Fermi's golden rule as *subradiant* [112,113]. In the case of GAs, it makes sense to use that term not only about collective emission, but also for a single atom, as the interference between its coupling points is analogous to the interference between many small atoms. A *perfectly subradiant* GA is one which does not decay into the bath. In this subsection, we first show how a GA can be perfectly subradiant with four coupling points, and how this subradiance is connected to a BIC. We then derive an analytical expression for this BIC and expand the discussion to various setups with more than four coupling points.

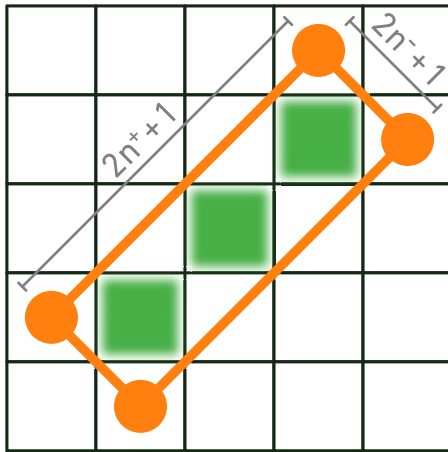


FIG. 2. A perfectly subradiant giant atom and its populated bound state in the continuum. The grid denotes the lattice of coupled cavities, with each square corresponding to one lattice site. The orange dots linked by a solid line denote the four coupling points of the giant atom. Note that the coupling points are separated by odd distances along each diagonal: $2n^+ + 1 = 3$ in the $\begin{bmatrix} 1 \\ 1 \end{bmatrix}$ direction and $2n^- + 1 = 1$ in the $\begin{bmatrix} 1 \\ -1 \end{bmatrix}$ direction. The green shading of lattice sites shows the evenly distributed photonic population of the bound state in the continuum, enclosed by the coupling points of the giant atom.

1. Subradiance and bound state in the continuum for a giant atom with four coupling points

In a 2D square lattice, a single GA can be perfectly subradiant if it has at least four coupling points. This is because it needs two points to interfere destructively and cancel the emission along each of the diagonals. Assuming all points couple with the same strength, achieving destructive interference requires the coupling points to be separated by an odd distance along each of the diagonals (see Fig. 2), since such a separation makes the excitations acquire a phase shift equal to an odd multiple of π when traveling between the coupling points. Conversely, an even distance between coupling points will lead to superradiance.

The interference between coupling points causing the subradiance of a GA is built through a *bound state in the continuum* (BIC). This is an eigenstate of the full Hamiltonian whose energy lies in the continuum, but does not interact with the propagating modes. The BIC is thus a *dressed state* of the system, whose photonic part is as a standing wave of localized excitations between the coupling points of the giant atom (see Fig. 2). The existence of such BICs has been previously reported for giant atoms in 1D [8,14,114] and 2D [28] structured environments, although often under different names, such as trapped emission or real pole.

The role of the BIC is clearly seen in the dynamics of the system (see Fig. 3). Starting with the atom in its bare excited state $|e\rangle$, we first observe a short decay that corresponds to the atom populating the photonic part of the BIC $|B\rangle$. During this time, which is the time it takes an excitation to travel through the bath and reach the other coupling points, there is also a small leakage into the environment, owing to the fact that the interference necessary for the subradiance has not yet been built. The excitation leaked away from the atom is approxi-

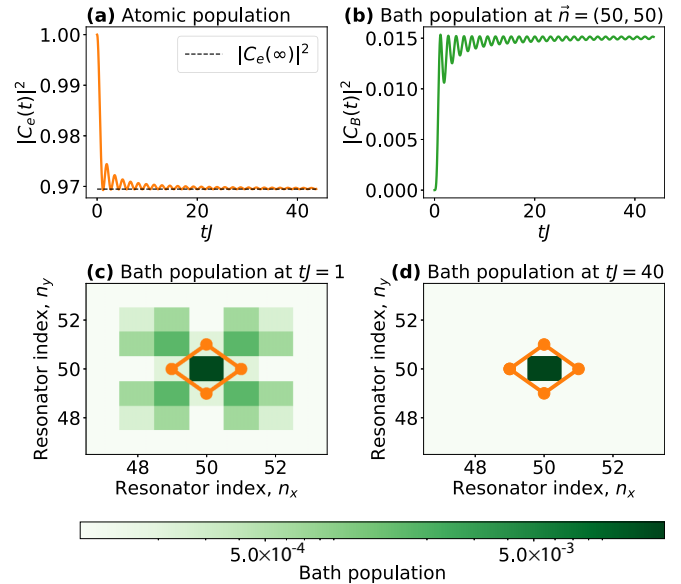


FIG. 3. Subradiant dynamics of a giant atom with four coupling points (orange markers connected by lines), all with coupling strength $g/J = 0.125$ ($G/J = 0.25$). The atom is tuned to the middle of the band ($\Delta/J = 0$) in a lattice of 100×100 coupled resonators. (a) Population of the atom, starting in the excited state and saturating at $|C_e(\infty)|^2$. (b) Population of the photonic part of the bound state, which corresponds to the only cavity enclosed by the coupling points of the atom. (c,d) Population of the bath in real space, at different times $tJ = 1, 40$.

mately equal to the excitation trapped in the photonic part of the BIC. This occurs because each coupling point should give off half of its emissions in the direction of another coupling point, and half along the diagonals pointing outward. After this decay, both the atom and the trapped excitation reach a nonradiative steady state: the BIC or dressed state. Note that in some experimental platforms, the leakage to the bath can be avoided by driving the dressed state (BIC) instead of the bare atomic excited state.

From resolvent formalism (see Appendix A), we know that the atomic steady-state population is given by [8,66]

$$\begin{aligned} |C_e(\infty)|^2 &= \left| \lim_{t \rightarrow \infty} \text{Res} \left[\frac{e^{-izt}}{z - \Delta - \Sigma_e(z)} \right] \right|^2 \\ &= \left| \frac{1}{1 - \partial_z \Sigma_e(z)|_{z=\Delta}} \right|^2, \end{aligned} \quad (21)$$

where z is the energy of the BIC and $\Sigma_e(z)$ is the self-energy of the atom. In particular, for a GA tuned to the middle of the band ($\Delta/J = 0$) with $P = 4$ coupling points and area $(2n^+ + 1) \times (2n^- + 1)$,

$$-\partial_z \Sigma_e(z)|_{z=0} = \frac{g^2}{J^2} (2n^+ + 1)(2n^- + 1). \quad (22)$$

In fact, it can be shown that in the single-excitation regime, the self-energy (and thus the time evolution) of a GA with coupling strength $g = g_0/\sqrt{4}$ is exactly the same as that of the state $|+\rangle = \frac{1}{2}(|eggg\rangle + |gegg\rangle + |ggge\rangle + |ggge\rangle)$ of a set of four small atoms with coupling strength g_0 coupled to the same points. This fact is quite intuitive from the derivation

of the effective coupling strength and Hamiltonian shown in Sec. III [see discussion around Eqs. (16)–(18)].

2. Analytical expression for the dressed excited state

Above we described the time evolution of the *bare* excited state of a perfectly subradiant GA, but here we derive a concise analytic expression for the *dressed* excited state, i.e., the eigenstate of the full Hamiltonian remaining stationary as $t \rightarrow \infty$. We consider the simplest perfectly subradiant configuration, with four coupling points surrounding a single photonic BIC peak, as seen in Fig. 3. Choosing the photonic BIC peak as the origin of our coordinate system and using notation where $|n\rangle$ is the state with an excitation present at the cavity with coordinate vector \vec{n} , we define

$$|B\rangle = \begin{bmatrix} 0 \\ 0 \end{bmatrix}, \quad (23)$$

$$|C\rangle = \left(\begin{bmatrix} 1 \\ 0 \end{bmatrix} + \begin{bmatrix} -1 \\ 0 \end{bmatrix} + \begin{bmatrix} 0 \\ 1 \end{bmatrix} + \begin{bmatrix} 0 \\ -1 \end{bmatrix} \right) / 2. \quad (24)$$

Inspired by what we observe in our numerical simulations in Fig. 3, we make the following ansatz for the dressed excited state:

$$|e'\rangle = \alpha|e\rangle + \beta|B\rangle, \quad (25)$$

where $|e\rangle$ is the bare excited state and $\alpha, \beta \in \mathbb{C}$. Applying H from Eq. (8) to this ansatz yields

$$\begin{aligned} H|e'\rangle &= \alpha H|e\rangle + \beta H|B\rangle = \{\Delta/J = 0\} \\ &= 2(\alpha g - \beta J)|C\rangle. \end{aligned} \quad (26)$$

Since $|e'\rangle$ is not proportional to $|C\rangle$, the only way for $|e'\rangle$ to be an eigenstate of the full Hamiltonian is if $\beta/\alpha = g/J$, making $|e'\rangle$ have eigenenergy 0. Normalization then gives that the dressed eigenstate for this perfectly subradiant GA is

$$|e'\rangle = \frac{1}{\sqrt{1 + g^2/J^2}} \left(|e\rangle + \frac{g}{J}|B\rangle \right). \quad (27)$$

This same derivation can be shown to hold for any perfectly subradiant configuration with only slight modifications. The main thing to note is that, in the general $\Delta/J = 0$ case, the $|B\rangle$ state needs to be defined with an alternating phase, related to how taking an odd number of steps along a diagonal in the lattice makes an excitation acquire a phase shift of π . For example, for the configuration in Fig. 2, one needs to use

$$|B\rangle = \left(\begin{bmatrix} 1 \\ 1 \end{bmatrix} - \begin{bmatrix} 0 \\ 0 \end{bmatrix} + \begin{bmatrix} -1 \\ -1 \end{bmatrix} \right) / \sqrt{3}, \quad (28)$$

so that $H|B\rangle$ only involves the cavities at the coupling points. In this case, when we have three photonic BIC peaks, the dressed excited state becomes

$$|e'\rangle = \frac{1}{\sqrt{1 + 3g^2/J^2}} \left(|e\rangle + \sqrt{3}\frac{g}{J}|B\rangle \right). \quad (29)$$

Finally, we note that these derivations can be extended to yield configurations of coupling points that avoid decoherence even when $\Delta/J \neq 0$ (see Appendix C). The BICs in such cases have a nature that is less atomic and more photonic [i.e., $|\langle e|e'\rangle|_{\Delta/J=0} > |\langle e|e'\rangle|_{\Delta/J \neq 0}$], in agreement with what has been observed in 1D [8].

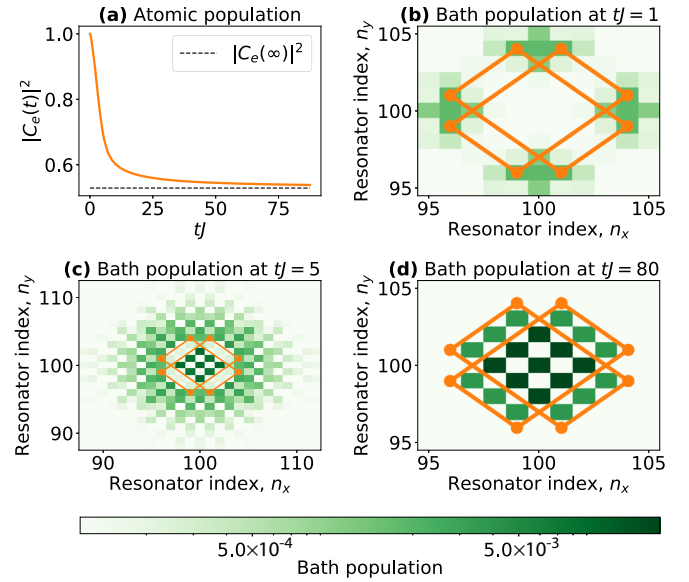


FIG. 4. Subradiant dynamics of a giant atom with eight coupling points (orange markers connected by lines), all with coupling strength $g/J = 0.088$ ($G/J = 0.25$). The atom is tuned to the middle of the band ($\Delta/J = 0$) in a lattice of 200×200 coupled resonators. (a) Population of the atom, starting in the excited state and saturating at $|C_e(\infty)|^2$. (b–d) Population of the bath in real space, at different times $tJ = 1, 5, 80$. Panel (d) shows a constructive interference between the photonic part of the bound states in the continuum of the two subradiant sets of coupling points.

3. Perfect subradiance with multiple sets of four coupling points

Beyond the minimal configurations with four coupling points discussed above, perfect subradiance can also be achieved by a GA with $P = 4p$ ($p \in \mathbb{N}$), where each set of four coupling points has the same coupling strength and is subradiant in itself. In such a case, the photonic BIC peaks generated by each set may interfere with the photonic BIC peaks from the other sets, either constructively (Fig. 4), destructively (Fig. 5), or not at all (Fig. 6). The interference pattern depends on the distribution of the coupling points, and arises from the alternating phase shown in Eq. (28).

For an analytical derivation of the interference patterns in the examples shown in Figs. 4–6, where $P = 8$, we consider the self-energy of the atom. It can be calculated as that of the two subradiant sets plus the interference between them:

$$\Sigma_e(z) = \Sigma_1(z) + \Sigma_2(z) + \Sigma_{\text{int}}(z). \quad (30)$$

Then, $\partial_z \Sigma_i(z)|_{z=0}$ is calculated as in Eq. (22), giving

$$-\partial_z \Sigma_{\text{int}}(z)|_{z=0} = \xi \frac{2g^2}{J^2} \cap^+ \cap^-, \quad (31)$$

where \cap^\pm is the overlap between the photonic BIC peaks generated by the two subsets along the $\begin{bmatrix} 1 \\ \pm 1 \end{bmatrix}$ diagonals and

$$\xi = \begin{cases} +1 & \text{constructive interference,} \\ 0 & \text{no interference,} \\ -1 & \text{destructive interference.} \end{cases} \quad (32)$$

In the particular case where both subsets of coupling points are centered around the same point in the bath (e.g., Figs. 4

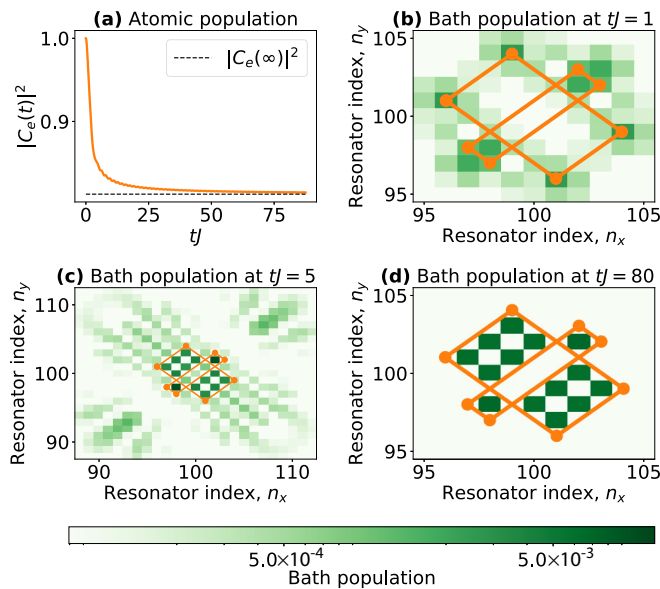


FIG. 5. Subradiant dynamics of a giant atom with eight coupling points (orange markers connected by lines), all with coupling strength $g/J = 0.088$ ($G/J = 0.25$). The atom is tuned to the middle of the band ($\Delta/J = 0$) in a lattice of 200×200 coupled resonators. (a) Population of the atom, starting in the excited state and saturating at $|C_e(\infty)|^2$. (b–d) Population of the bath in real space, at different times $tJ = 1, 5, 80$. Panel (d) shows a destructive interference between the photonic part of the bound states in the continuum of the two subradiant sets of coupling points.

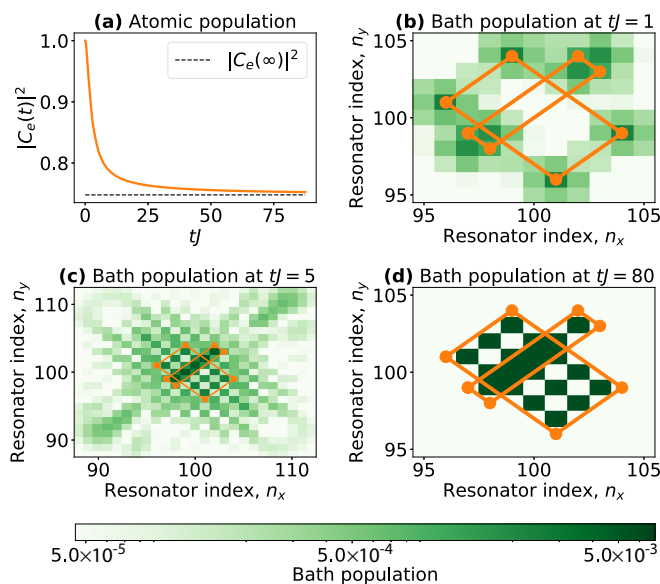


FIG. 6. Subradiant dynamics of a giant atom with eight coupling points (orange markers connected by lines), all with coupling strength $g/J = 0.088$ ($G/J = 0.25$). The atom is tuned to the middle of the band ($\Delta/J = 0$) in a lattice of 200×200 coupled resonators. (a) Population of the atom, starting in the excited state and saturating at $|C_e(\infty)|^2$. (b–d) Population of the bath in real space, at different times $tJ = 1, 5, 80$. Panel (d) shows no interference between the photonic part of the bound states in the continuum of the two subradiant sets of coupling points.

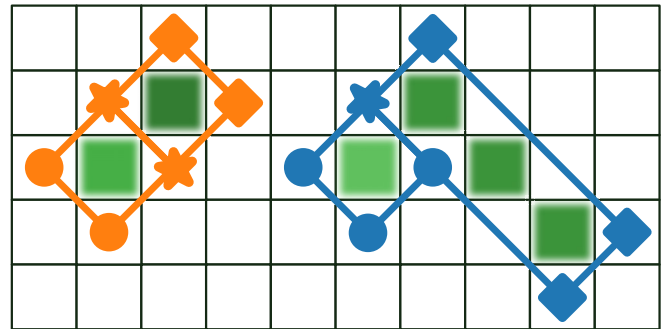


FIG. 7. Two perfectly subradiant giant atoms with a number of coupling points that is not a multiple of four. The orange and blue marks linked by a solid line denote the coupling points of each atom, respectively. The circles indicate points with coupling strength g_1 , the squares indicate points with strength $g_2 > g_1$, and the stars couple with strength $g_1 + g_2$. The green lattice sites show the photonic excitation of the bound state in the continuum, with the intensity of the color referring to the population on each site (darker color indicates higher population).

and 5),

$$\begin{aligned} \cap^+ &= 2 \min(n_1^+, n_2^+) + 1, \\ \cap^- &= 2 \min(n_1^-, n_2^-) + 1, \\ \xi &= (-1)^{n_1^+ + n_2^+ + n_1^- + n_2^-}. \end{aligned} \quad (33)$$

We highlight that, to the best of our knowledge, this interference between the photonic components of different BICs has not been reported before.

4. Other perfectly subradiant configurations of coupling points

One can also achieve perfectly subradiant configurations with $P \neq 4p$ by superimposing subradiant setups with four coupling points in such a way that some coupling points end up on top of one another. Each set of overlapping coupling points can then be replaced with a single coupling point, whose coupling strength equals the sum of the coupling strengths of the overlapping points. For example, two superimposed coupling points with coupling strengths g_1 and g_2 would be replaced by a single coupling point with coupling strength $g = g_1 + g_2$, as shown in Fig. 7. We note that this additive property for coupling points also holds if we allow negative (or complex) coupling strengths.

B. Multiple giant atoms—Decoherence-free interaction

Unlike small atoms, GAs can interact without decohering when tuned to the continuum. This is one of the most intriguing, and potentially useful, properties of GAs; it has been reported in 1D continuous waveguides [4–7,9,115] and 1D structured waveguides [8,54]. Here, we show how such decoherence-free interaction (DFI) between GAs is also possible in 2D, and how it differs from the interaction outside the continuum (i.e., in the band gap), which is also possible for small atoms. We first consider two GAs and then also explore how many GAs can have pairwise DFI in various configurations.

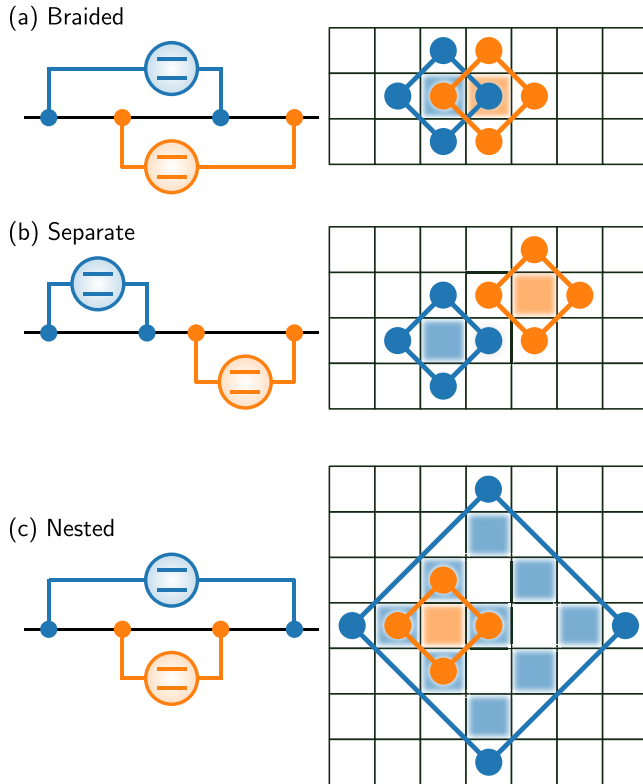


FIG. 8. Analogy between the different configurations of giant atoms coupled to a 1D waveguide (left) and to a 2D square lattice (right). Left, 1D: the black line represents the waveguide. The two atoms (blue and orange) are coupled to it at the points marked by the blue and orange dots, respectively. Right, 2D: The grid denotes the lattice of coupled cavities, with each square corresponding to one lattice site. The blue (orange) dots united by a continuous line denote the four coupling points of the first (second) giant atom. The blue (orange) lattice sites show the photonic part of the bound states in the continuum of the blue (orange) atom. These parts mediate the decoherence-free interaction if the orange (blue) atom has a coupling point on a blue (orange) lattice site and vice versa. (a) Braided configuration—the only one that allows decoherence-free interaction. (b) Separate configuration. (c) Nested configuration.

Outside the continuum, it is well known that atom-photon bound states are formed, with photons becoming exponentially localized in the vicinity of the atoms (small or giant), thus inhibiting their decay [8,66,116]. Furthermore, multiple atoms coupled to the same reservoir can interact through the overlap of their bound-state photonic wave functions [117–119], and since the atoms are decoupled from the propagating modes, this interaction is inherently decoherence-free.

We find that the interaction mechanism in the continuum is not quite the same: for DFI to take place, each of the GAs need to be perfectly subradiant and have at least one of their coupling points in a cavity populated by a BIC associated with the other atom (see Fig. 8). Note that this mechanism also applies to 1D structured waveguides, although that has not been reported before with such clarity. In fact, for two GAs, this configuration is analogous to the so-called *braided* one in 1D [4,8], which is typically the only one allowing DFI.

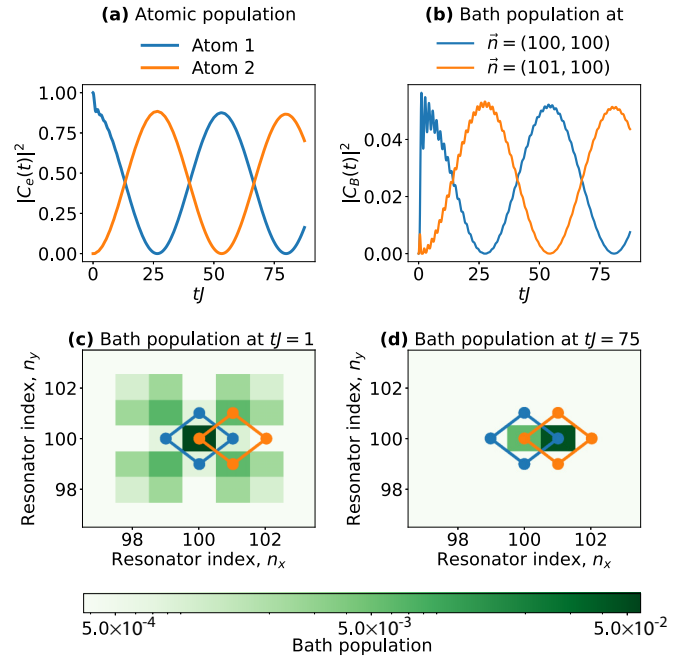


FIG. 9. Decoherence-free dynamics of two giant atoms with four coupling points each (blue and orange dots linked by solid lines), all with coupling strength $g/J = 0.25$ ($G/J = 0.5$). The atoms are tuned to the middle of the band ($\Delta/J = 0$), in a lattice of 200×200 coupled resonators. (a) Population of the atoms, starting in the bare excited state of atom 1. The different regimes and contributions to the dynamics are explained in Sec. IV B 1. (b) Population of the photonic parts of bound states 1 (blue) and 2 (orange), i.e., of the cavities enclosed by atoms 1 and 2, respectively. (c, d) Population of the bath in real space, at different times $tJ = 1, 75$.

Similarly to 1D, 2D configurations analogous to the *nested* and *separate* ones (see Fig. 8) do not allow for DFI either.

1. Two giant atoms

In Fig. 9, we depict the canonical signature of DFI, i.e., the time evolution of two braided GAs exchanging an excitation back and forth. We note that this evolution is nearly identical to that in 1D [8]: starting with the first atom in its bare excited state, there is an initial exponential decay corresponding to the buildup of the interference, for a time

$$\tau = \frac{d}{v_g} = \frac{2 \max(n^+, n^-) + 1}{2J}, \quad (34)$$

which is then followed by weakly damped population exchanges $[\cos^2(z_R t) e^{-2z_I t}]$. As shown in the 1D case [8], the interaction rate z_R is given by the real part of the energy of the two BICs ($z_R = |\text{Re}(z_1) - \text{Re}(z_2)|/2$), whereas the damping rate is given by the imaginary part ($z_I = |\text{Im}(z_1) + \text{Im}(z_2)|/2$). Note that the damping, which occurs due to a combination of the retardation effects and the exchange interaction being nonzero, makes these states *quasibound*. We refer the interested reader to Ref. [8] for an in-depth discussion on the factors that influence the interaction strength and quality of the DFI population exchanges.

Finally, we identify the Rabi swaps between the photonic parts of the bound states (Fig. 9, top right panel) as the two-

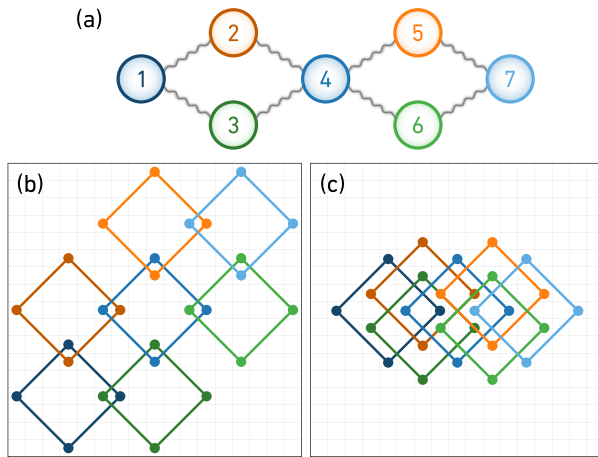


FIG. 10. Decoherence-free braided chains of seven giant atoms. The subchain formed by atoms 1-2-4-5-7 (i.e., without the green atoms) is also a DFI braided chain. (a) Sketch of the connections between the seven atoms. Gray squiggly lines denote atoms that interact with each other without decohering. (b, c) Two possible implementations of the chain shown in (a) with seven atoms having four coupling points each, tuned to the middle of the band ($\Delta/J = 0$). The dots linked by a solid line denote the four coupling points of each giant atom. (b) Loosely braided. (c) Tightly braided. Note that even if atoms 2-5, 1-4-7, and 3-6 also seem to be braided, they do not directly interact with each other, since none of their coupling points connect to a cavity containing some photonic part of the bound state in the continuum of the other atom(s).

atom analog of the so-called *oscillating BICs* [10–14,54]. The latter have been shown to appear in GAs with three or more coupling points to the waveguide (continuous or structured), where multiple BIC solutions coexist and give rise to dynamic oscillations. In the 2D setups we study here, the multiplicity of BICs does not come from the multiplicity of coupling points, but instead, from the multiplicity of atoms.

2. Many giant atoms

As one may suspect, DFI is also possible beyond two GAs in decoherence-free chains with pairwise interaction (reported before in 1D for continuous waveguides [4,7]). Many configurations of such chains, both 1D and 2D, are feasible to transport excitations, as shown in Fig. 10.

Moreover, these GAs allow *all-to-all interaction*, which is possible in 1D continuous waveguides in the minimal configuration (i.e., three GAs having two coupling points each) [4]. In the 2D square lattice, however, the minimal configuration of three GAs with four coupling points each does not suffice, and achieving all-to-all interaction requires additional coupling points. For example, in Fig. 11, we show a layout of three GAs with eight coupling points each, in which all atoms are perfectly subradiant, and each atom has at least one coupling point fully surrounded by each of the other atoms.

Finally, without having all-to-all interaction, we can still build high-connectivity grids with GAs that just have four coupling points each, like the arrangement shown in Fig. 12. In this example, we establish long-range DFI between distant atoms that are mediated by a bath containing only nearest-neighbor couplings. This kind of setup could prove useful

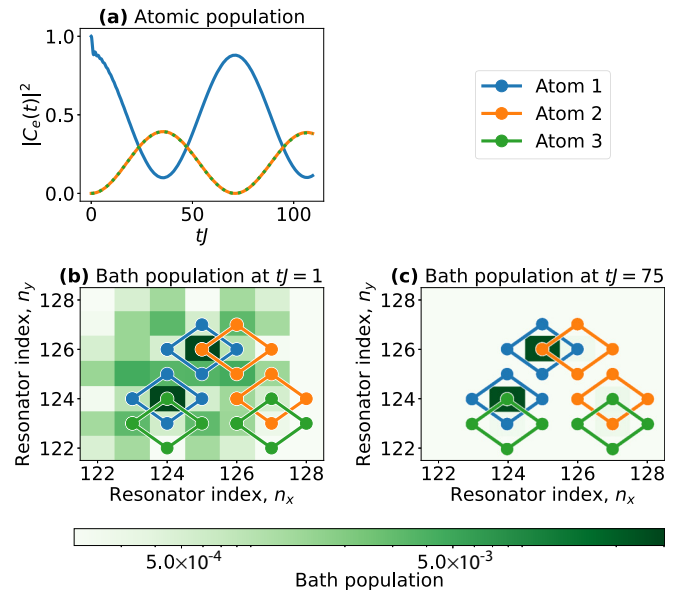


FIG. 11. All-to-all interaction between three giant atoms with eight coupling points each, all with coupling strength $g/J = 0.177$ ($G/J = 0.5$). The atoms are tuned to the band ($\Delta/J = 0$) in a lattice of 250×250 coupled resonators. (a) Population of the atoms, starting in the bare excited state of atom 1. The different regimes and contributions to the dynamics are explained in Sec. IV B 1. (b, c) Population of the bath in real space, at different times $tJ = 1, 75$. The blue (atom 1), orange (atom 2), and green (atom 3) markers linked by solid lines of the same color indicate the sets of coupling points that are in a perfectly subradiant configuration.

in quantum simulation of systems beyond nearest-neighbor interaction [102,120–122], as well as in the implementation of nonlocal quantum gates.

V. CONCLUSION

We conducted a detailed theoretical study of giant atoms (GAs) in 2D structured environments. We focused on the case when this environment is a square lattice of cavities, which

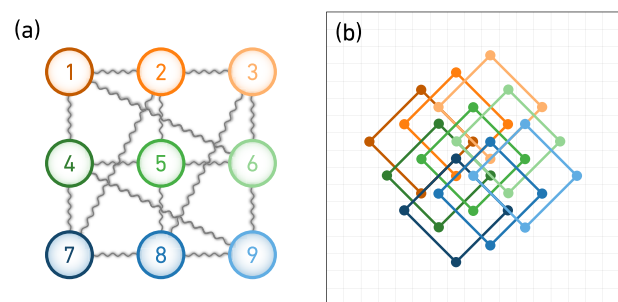


FIG. 12. High-connectivity grid of nine identical giant atoms (the different colors are for readability). (a) Sketch of the connections between the nine atoms. Gray squiggly lines denote atoms that interact with each other without decohering. (b) A possible implementation of the grid shown in (a) with nine giant atoms having four coupling points each, tuned to the middle of the band ($\Delta/J = 0$). The dots linked by a solid line denote the four coupling points of each atom.

leads to band gaps and an energy band that comes with an anisotropic energy dispersion at its center. In this setting, we showed how GAs can avoid relaxing into the environment.

For a single GA with a transition frequency in the center of the band, we found that it can display perfect subradiance, i.e., completely suppressed emission of energy into the environment, if the atom couples to the bath through at least four cavities. This suppression is because the propagation of excitations in the environment is restricted to be diagonal at the band center; with four coupling points it becomes possible to cancel emission along these four propagation directions through destructive interference between the emissions from pairs of coupling points. We also showed that such perfect subradiance can be achieved with more coupling points, if their number is a multiple of four and the coupling strength is equal at all coupling points. Allowing for coupling strengths to vary between coupling points (including becoming negative), we further showed how subradiance can be achieved in setups with other numbers of coupling points, both even and odd.

For multiple GAs, we showed that the concept of decoherence-free interaction (DFI; two GAs interacting through an environment without losing energy into that environment), previously demonstrated in a 1D setting, also can be realized in 2D. More specifically, we showed that this DFI can take place if the individual atoms have their coupling points arranged to be subradiant and each atom has some (but not all) of its coupling points enclosed by coupling points from the other atom. This setup constitutes a generalization of the so-called braided setup of coupling points required for GAs in 1D [4,8]. We further showed how this DFI for GAs in 2D can be extended to more atoms, forming effective high-connectivity (even all-to-all coupling) lattices of atoms connected through DFI.

The results we found for both single and multiple GAs can be understood as manifestations of bound states in the continuum (BICs). For a single GA in a subradiant configuration, an initial excitation in the atom mostly remains there. A small amount of energy leaks into the environment outside the atom before the destructive interference between emissions from the different coupling points kicks in, but about half that energy remains in the photonic part of a BIC formed in-between the coupling points of the atom. For multiple GAs, DFI between pairs of them is only possible when some coupling point(s) of each atom in the pair are placed in locations that contain a part of the BIC associated with the other atom.

We note that these results were enabled by nontrivial extensions of analytical and numerical methods previously employed to study small atoms in 2D structured environments. Through these extensions, we were able to obtain analytical expressions for the steady-state populations of GAs and their BICs, and perform numerical simulations of how the atomic and photonic populations evolve in time for both single and multiple GAs. For DFI between a pair of GAs, we observed that both the atomic populations and the photonic parts of the BIC populations undergo Rabi oscillations when one of the atoms is initialized in its excited state and the rest of the system is initialized in its ground state.

As we discuss at the end of Sec. II, the effects revealed in this study should be possible to observe with existing technology in several experimental platforms. We believe that

a setup with superconducting qubits coupled to a lattice of microwave resonators seems most promising for such experimental demonstrations. We note that arranging for the multiple coupling points in such a setup may be aided by flip-chip technology [104–106].

The properties of GAs in 2D structured environments that we have discussed in this paper may find applications in quantum computing and quantum simulation. In these fields, the ability to protect qubits from decoherence while at the same time enabling them to interact, preferably with a high connectivity, is crucial, and we have shown that the DFI between GAs in 2D provides such capability. In particular, the DFI between GAs may be especially interesting for simulation of open quantum systems, since the interaction of the atoms with the environment can be turned on and off by tuning the atomic frequency, which is possible, e.g., with superconducting qubits [5,123].

There are several possible directions for future work. Beyond more detailed studies of the possible applications discussed in the preceding paragraph, one could study other 2D lattices than the square grid or introduce varying hopping rates between the cavities in such a lattice. Such changes could lead to other band structures, including ones with topological properties. Given the importance of BICs and subradiance, it would also be interesting to extend the model to more than one excitation to study superradiance and multiphoton BICs. It may furthermore be valuable to consider more than two energy levels in each GA, since additional atomic levels are crucial in several quantum-optics effects.

ACKNOWLEDGMENTS

We thank Alberto del Ángel, Simon Pettersson Fors, Théo Sépulcre, and Alejandro González-Tudela for useful discussions. We acknowledge support from the Swedish Research Council (Grant No. 2019-03696), from the Knut and Alice Wallenberg Foundation through the Wallenberg Centre for Quantum Technology (WACQT), and from the Swedish Foundation for Strategic Research (Grants No. FFL21-0279 and No. FUS21-0063).

APPENDIX A: RESOLVENT FORMALISM

The formalism used here is based on Chap. 3 of Ref. [124] and adapted to the particular case of giant atoms (GAs) coupled to a 2D square lattice through P coupling points. For the 1D structured waveguide case, see the derivation in Ref. [8].

1. A single giant atom—Derivation of the self-energy and probability amplitude

We consider the total Hamiltonian of a single GA coupled to a structured lattice from Eq. (8), $H = H_0 + H_{\text{int}}$, where

$$H_0 = H_A + H_B = \Delta\sigma^+\sigma^- + \sum_k \omega(k)a_k^\dagger a_k, \quad (\text{A1})$$

$$H_{\text{int}} = \sum_{p=1}^P \frac{g_p}{N} \sum_{\vec{k}} (e^{-i\vec{k}\cdot\vec{n}_p} a_{\vec{k}} \sigma^+ + \text{H.c.}), \quad (\text{A2})$$

In the single-excitation subspace, the eigenstates of the bare Hamiltonian H_0 are $|e\rangle := |e, 0\rangle$ and $|\vec{k}\rangle := |g, \vec{k}\rangle$, for $\vec{k} = (k_x, k_y)$ and $k_x, k_y \in \{-\pi, \dots, \pi - \frac{2\pi}{N}\}$. The interaction term

H_{int} couples these atomic and photonic subspaces $\{|e\rangle\}$ and $\{|\vec{k}\rangle\}$ to one another.

The *resolvent* of the Hamiltonian is defined by

$$G(z) = \frac{1}{z - H}. \quad (\text{A3})$$

In general, for a projection \mathcal{P} onto a subset spanned by a set of eigenvectors of H_0 and its complement $\mathcal{Q} = 1 - \mathcal{P}$, the resolvent obeys

$$\mathcal{P}G(z)\mathcal{P} = \frac{\mathcal{P}}{z - \mathcal{P}H_0\mathcal{P} - \mathcal{P}\Sigma(z)\mathcal{P}}, \quad (\text{A4})$$

where

$$\begin{aligned} \Sigma(z) &= H_{\text{int}} + H_{\text{int}} \frac{\mathcal{Q}}{z - \mathcal{Q}H_0\mathcal{Q} - \mathcal{Q}H_{\text{int}}\mathcal{Q}} H_{\text{int}} \\ &\approx H_{\text{int}} + H_{\text{int}} \frac{\mathcal{Q}}{z - H_0} H_{\text{int}} \end{aligned} \quad (\text{A5})$$

is the *level-shift operator*. Note that the approximation symbol above denotes the second-order perturbative expansion in powers of H_{int} , a truncation that is justified since H_{int} is small compared to H_0 . In particular, when \mathcal{P} is the projector onto a single state $|\alpha\rangle$ with energy E_α ,

$$G_\alpha(z) = \frac{1}{z - E_\alpha - \Sigma_\alpha(z)}, \quad (\text{A6})$$

with $G_\alpha(z) = \langle \alpha | G(z) | \alpha \rangle$ and $\Sigma_\alpha(z) = \langle \alpha | \Sigma(z) | \alpha \rangle$.

In our case, we define $\mathcal{P} = |e\rangle\langle e|$ and its complement $\mathcal{Q} = \sum_{\vec{k}} |\vec{k}\rangle\langle \vec{k}|$. Then we can write the self-energy of the atom $\Sigma_e(z) = \langle e | \Sigma(z) | e \rangle$ as follows:

$$\begin{aligned} \Sigma_e(z) &= \langle e | H_{\text{int}} | e \rangle + \sum_{\vec{k}} \langle e | H_{\text{int}} \frac{|\vec{k}\rangle\langle \vec{k}|}{z - H_0} H_{\text{int}} | e \rangle \\ &= \frac{1}{N^2} \sum_{\vec{k}} \frac{(\sum_p g_p e^{-i\vec{k}\cdot\vec{n}_p}) (\sum_q g_q^* e^{i\vec{k}\cdot\vec{n}_q})}{z - \omega(\vec{k})}. \end{aligned} \quad (\text{A7})$$

Henceforth, we use the dispersion relation $\omega(\vec{k}) = -2J[\cos(k_x) + \cos(k_y)]$ and that the distance vector between two different coupling points is $\Delta\vec{n}$. For simplicity, let us also assume that $g_p = g_q = g \in \mathbb{R}$. Then,

$$\Sigma_e(z) = \frac{g^2}{N^2} \sum_{\vec{k}} \frac{P + 2 \sum_{\Delta\vec{n}} \cos(\vec{k} \cdot \Delta\vec{n})}{z + 2J[\cos(k_x) + \cos(k_y)]}. \quad (\text{A8})$$

In the continuum limit, i.e., when $N \rightarrow \infty$, the sum over \vec{k} becomes a double integral: $\sum_{\vec{k}} \left(\frac{2\pi}{N}\right)^2 \rightarrow \iint_{\vec{k}} d^2\vec{k}$. Therefore, we can write the self-energy as

$$\begin{aligned} \Sigma_e(z) &\rightarrow \frac{g^2}{(2\pi)^2} \iint_{-\pi}^{\pi} d^2\vec{k} \frac{P + 2 \sum_{\Delta\vec{n}} \cos(\vec{k} \cdot \Delta\vec{n})}{z + 2J[\cos(k_x) + \cos(k_y)]} \quad (\text{A9}) \\ &= P \underbrace{\frac{g^2}{(2\pi)^2} \iint_{-\pi}^{\pi} d^2\vec{k} \frac{1}{z + 2J[\cos(k_x) + \cos(k_y)]}}_{\Sigma_{\text{SA}}(z)} \\ &\quad + 2 \sum_{\Delta\vec{n}} \underbrace{\frac{g^2}{(2\pi)^2} \iint_{-\pi}^{\pi} d^2\vec{k} \frac{\cos(\vec{k} \cdot \Delta\vec{n})}{z + 2J[\cos(k_x) + \cos(k_y)]}}_{\Sigma_{\Delta\vec{n}}(z)}, \end{aligned} \quad (\text{A10})$$

where the self-energy of a small atom $\Sigma_{\text{SA}}(z)$ is calculated from the particular case of a GA [Eq. (A9)] with $P = 1$ (and therefore $\Delta\vec{n} = 0$, since there is only one coupling point); and $\Sigma_{\Delta\vec{n}}(z)$ denotes the contribution to the self-energy from the interference between coupling points that are spaced by $\Delta\vec{n}$. For example, consider the diamond configuration shown in Fig. 3. The self-energy of the atom in such a case, according to Eq. (A10), is

$$\Sigma_\diamond(z) = 4\Sigma_{\text{SA}}(z) + 2 \left[4\Sigma_{\begin{bmatrix} 1 \\ 1 \end{bmatrix}}(z) + 2\Sigma_{\begin{bmatrix} 2 \\ 0 \end{bmatrix}}(z) \right]. \quad (\text{A11})$$

As shown in Ref. [125], it is convenient to rewrite Σ_{SA} and $\Sigma_{\Delta\vec{n}}$ in a different basis, such that instead of integrating in the $k_{x,y}$ horizontal and vertical directions, we integrate in the q_\pm diagonal directions. For that, we apply the following change of variables:

$$q_\pm = \frac{1}{2}(k_x \pm k_y), \quad (\text{A12})$$

$$\Delta n_\pm = \Delta n_x \pm \Delta n_y. \quad (\text{A13})$$

Note that this implies $d^2\vec{q} = \frac{1}{2}d^2\vec{k}$ and that the integration area in the $k_{x,y}$ direction is twice the area of that in the q_\pm direction. Using the trigonometric expressions $\cos(\alpha \pm \beta) = \cos(\alpha)\cos(\beta) \mp \sin(\alpha)\sin(\beta)$ and $\cos(2\alpha) = 2\cos^2(\alpha) - 1 = 1 - 2\sin^2(\alpha)$, we can show that

$$\begin{aligned} \Sigma_{\text{SA}}(z) &= \frac{g^2}{(2\pi)^2} \iint_{-\pi}^{\pi} d^2\vec{k} \frac{1}{z + 2J[\cos(k_x) + \cos(k_y)]} \\ &= \frac{g^2}{(2\pi)^2} \iint_{-\pi}^{\pi} d^2\vec{q} \frac{1}{z + 4J\cos(q_+) \cos(q_-)}, \quad (\text{A14}) \\ \Sigma_{\Delta\vec{n}}(z) &= \frac{g^2}{(2\pi)^2} \iint_{-\pi}^{\pi} d^2\vec{k} \frac{\cos(\vec{k} \cdot \Delta\vec{n})}{z + 2J[\cos(k_x) + \cos(k_y)]} \\ &= \frac{g^2}{(2\pi)^2} \iint_{-\pi}^{\pi} d^2\vec{q} \frac{\cos(q_+ \Delta n_+) \cos(q_- \Delta n_-)}{z + 4J\cos(q_+) \cos(q_-)}. \end{aligned} \quad (\text{A15})$$

In this basis, the expressions above can be integrated by parts and rewritten in a compact way in terms of elliptic integrals [125]. For instance, from Ref. [66]:

$$\Sigma_{\text{SA}}(z) = \frac{2g^2}{\pi z} K[m(z)], \quad (\text{A16})$$

$$\Sigma_{\begin{bmatrix} 1 \\ 1 \end{bmatrix}}(z) = \frac{2g^2}{\pi z} \left\{ \left[\frac{2}{m(z)} - 1 \right] K[m(z)] - \frac{2}{m(z)} E[m(z)] \right\}, \quad (\text{A17})$$

$$\Sigma_{\begin{bmatrix} 1 \\ 0 \end{bmatrix}}(z) = \frac{g^2}{4J} - \frac{g^2}{2\pi J} K[m(z)], \quad (\text{A18})$$

where

$$m(z) = \left(\frac{4J}{z} \right)^2, \quad (\text{A19})$$

and K and E are the complete elliptical integrals of the first and second kind, respectively:

$$K(m) = \int_0^{\pi/2} \frac{d\phi}{\sqrt{1 - m \sin^2(\phi)}}, \quad (\text{A20})$$

$$E(m) = \int_0^{\pi/2} d\phi \sqrt{1 - m \sin^2(\phi)}. \quad (\text{A21})$$

Finally, using the recursive formulas in Ref. [125], we can obtain the self-energy at any arbitrary site. For example, using

$$\begin{aligned} \Sigma_{[m+1]}(z) = & -\frac{1}{2J} \left[2z \Sigma_{[m]}(z) + 2J \Sigma_{[m-1]}(z) \right. \\ & \left. + 4J \Sigma_{[m]}(z) \right], \end{aligned} \quad (\text{A22})$$

together with Eqs. (A16)–(A17), we can show that

$$\begin{aligned} \Sigma_{[2]}(z) = & -\frac{z}{J} \Sigma_{[1]}(z) - \underbrace{\Sigma_{[0]}(z)}_{\Sigma_{\text{SA}}(z)} - 2\Sigma_{[1]}(z) \\ = & \frac{2g^2}{\pi z} \left(K[m(z)] + \frac{4}{m(z)} \left\{ E[m(z)] - \frac{\pi}{2} \right\} \right). \end{aligned} \quad (\text{A23})$$

Going back to the diamond configuration [Eq. (A11)], we have now derived an expression for the self-energy that is integrable in the first Riemann sheet, i.e., $|z| > 4J$. Then, according to Eq. (A6), the resolvent-operator element corresponding to the excited state of the atom is

$$G_e(z) = \frac{1}{z - \Delta - \Sigma_e(z)}, \quad (\text{A24})$$

with Δ the atom-cavity detuning. Last, we can express the probability amplitude of an initially excited GA, for $t > 0$, as follows:

$$C_e(t) = -\frac{1}{2\pi i} \int_{-\infty}^{\infty} G_e(E + i0^+) e^{-iEt} dE, \quad (\text{A25})$$

i.e., as the Fourier transform of the retarded Green's function G_e .

2. Integration contour of the probability amplitude

Similarly to the 1D coupled-cavity array, the energy dispersion of the 2D square lattice introduces branch cuts at the band edges, making the integral in Eq. (A25) contour around them (see Fig. 13). Moreover, an additional branch point that is not present in the 1D case arises in the middle of the band due to the additional van Hove singularity. Therefore, the branch cuts divide the surface enclosed by the contour into three Riemann sheets: the first Riemann sheet corresponds to the energy values outside the band ($|z| > 4J$) and contains real poles of the Green's function [Eq. (A24)], which are associated to the atom-photon bound states; while the second ($-4J < z < 0$) and third ($0 < z < 4J$) Riemann sheets extend over the band and contain the complex poles of the Green's function, which are responsible for the spontaneous emission into the bath.

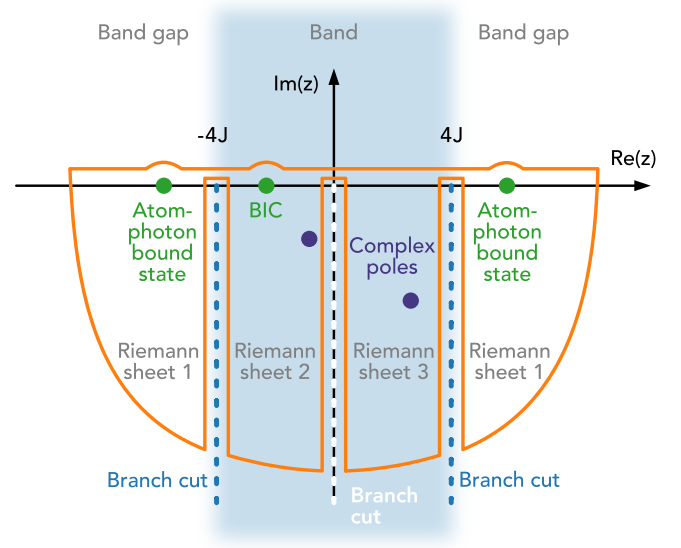


FIG. 13. Contour of the integral in Eq. (A25), with contributions from the poles of the Green's function [Eq. (A24)], as well as the branch cuts at the band edges and at the middle of the band.

The poles in the second and third Riemann sheets that are real are responsible for the existence of the bound states in the continuum (BICs).

Essentially, this means that the atomic population $|C_e(t)|^2$ is affected by two elements: detours around the branch cuts and poles of the Green's function. In fact, as explained in Refs. [8,66], the probability amplitude $C_e(t)$ can be calculated as a sum of the different contributions:

$$C_e(t) = \sum_{\alpha \in \text{branch cuts}} C_\alpha(t) + \sum_{\beta \in \text{poles}} R_\beta e^{-iz_\beta t}, \quad (\text{A26})$$

where C_α has the form of Eq. (A25), and R_β is the residue of the poles (real and complex) that we obtain through the residue theorem, which is the overlap of the initial wave function with the poles, i.e.,

$$R_\beta = \frac{1}{1 - \partial_z \Sigma_e(z)} \Big|_{z=z_\beta}. \quad (\text{A27})$$

The singularities that give rise to the branch cuts not only affect the contour of the probability-amplitude integral, but also limit the domain of definition of the self-energy. In fact, the expressions given in Eqs. (A16)–(A18) and Eq. (A23) are only valid for the first Riemann sheet. The analytical continuation into the second and third Riemann sheets can be obtained by transforming the elliptical integrals in the following way [66]:

$$K^{\text{III}}(m) = K(m) \pm 2iK(1 - m), \quad (\text{A28})$$

$$E^{\text{III}}(m) = E(m) \pm 2i[K(1 - m) - E(1 - m)]. \quad (\text{A29})$$

APPENDIX B: EFFICIENT COMPUTATION OF THE TIME-EVOLUTION OPERATOR U_A FOR GIANT ATOMS

As outlined in Sec. III, the time evolution generated by the atom-interaction Hamiltonian

$$H_A + H_{\text{int}} = \begin{bmatrix} D & \Gamma \\ \Gamma^T & \mathbb{0} \end{bmatrix} \quad (\text{B1})$$

can be modeled efficiently by using M different effective Hamiltonians H_i , each modeling the interaction between one of the atoms and the bath. In the GA case, the D matrix still looks the same as in the small-atom case: $D_{ij} = \Delta_i \delta_{ij}$. However, Γ looks slightly different:

$$[\Gamma]_{in} = \begin{cases} g_{ip_n} & \text{if atom } i \text{ couples to cavity } n, \\ 0 & \text{otherwise,} \end{cases} \quad (\text{B2})$$

where p_n is the point index corresponding to the coupling point at cavity n .

In this Appendix, we show the details of how this efficient modeling can be done by deriving Eq. (20) from how $H_A + H_{\text{int}}$ behaves when exponentiated. For simplicity, we henceforth refer to $H_A + H_{\text{int}}$ as H in this Appendix, since we will not need to refer to the full Hamiltonian $H_B + H_A + H_{\text{int}}$ much. The reason that understanding the structure of H^k is a good place to start is that by definition

$$U_A(\Delta t) = e^{-iH\Delta t} = \sum_{k \geq 0} \frac{(-i\Delta t)^k}{k!} H^k, \quad (\text{B3})$$

so knowing how H^k looks should (and indeed does) enable us to find explicit expressions for the matrix elements of $U_A(\Delta t)$ —namely, those of Eq. (20).

Computing H^k explicitly for $k = 0$ and $k = 1$ is trivial: $H^0 = \mathbb{1}$ and $H^1 = H$. For the first nontrivial case, $k = 2$, we find that

$$H^2 = \begin{bmatrix} D^2 + \Gamma\Gamma^T & D\Gamma \\ \Gamma^T D & \Gamma^T \Gamma \end{bmatrix}. \quad (\text{B4})$$

Since D is diagonal, so is D^2 —specifically,

$$[D^2]_{ij} = \Delta_i^2 \delta_{ij}. \quad (\text{B5})$$

Examining the definition of Γ leads us to the conclusion that $\Gamma\Gamma^T$ is also diagonal:

$$\begin{aligned} [\Gamma\Gamma^T]_{ij} &= \sum_{n=1}^{N^2} \Gamma_{in} \Gamma_{jn} \\ &= \text{no cavity couples to } > 1 \text{ atom} \\ &= \sum_{p=1}^{P_i} g_{ip}^2 \delta_{ij}, \end{aligned} \quad (\text{B6})$$

Introducing the notation Λ_k for the top-left ("atomic") block of H^k , so that $\Lambda_1 = D$ and $\Lambda_0 = \mathbb{1}$, we see that Λ_2 , the top-left block of H^2 , is still diagonal, with elements

$$[\Lambda_2]_{ij} = (\Delta_i^2 + G_i^2) \delta_{ij}, \quad (\text{B7})$$

if we define the effective coupling strength

$$G_i = \sqrt{\sum_{p=1}^{P_i} g_{ip}^2}. \quad (\text{B8})$$

If we instead take a look at the top-right block, then we see that since D is diagonal,

$$[D\Gamma]_{in} = \begin{cases} \Delta_i g_{ip_n} & \text{if atom } i \text{ couples to cavity } n, \\ 0 & \text{otherwise.} \end{cases} \quad (\text{B9})$$

Thus, the structure of this block also remains the same—squaring H simply results in the nonzero matrix elements contained therein changing from g_{ip_n} to $\Delta_i g_{ip_n}$. Since H is symmetric (recalling the assumption we made for calculational convenience that all coupling strengths g_{ip} are real), the bottom-left block is simply the transpose of the top-right.

Finally, the bottom-right block of H^2 has matrix elements

$$\begin{aligned} [\Gamma^T \Gamma]_{mn} &= \sum_{i=1}^M \Gamma_{im} \Gamma_{in} \\ &= \{\text{no cavity couples to } > 1 \text{ atom}\} \\ &= \begin{cases} g_{ip_m} g_{ip_n} & \text{if atom } i \text{ couples cavities } m \text{ and } n, \\ 0 & \text{otherwise.} \end{cases} \end{aligned} \quad (\text{B10})$$

Note that all of the elements in the four blocks involve only a single atom each, which means that the time evolution caused by U_A to one atom can be treated independently from all the others, just as we noted in Sec. III.

Examining the case $k = 3$, we find

$$\begin{aligned} H^3 &= \begin{bmatrix} D\Lambda_2 + \Gamma\Gamma^T \Lambda_1 & \Lambda_2 \Gamma \\ \Gamma^T \Lambda_2 & \Gamma^T \Lambda_1 \Gamma \end{bmatrix} \\ &= \begin{bmatrix} D^3 + 2\Gamma\Gamma^T D & (D^2 + \Gamma\Gamma^T) \Gamma \\ \Gamma^T (D^2 + \Gamma\Gamma^T) & \Gamma^T D \Gamma \end{bmatrix}. \end{aligned} \quad (\text{B11})$$

A pattern starts to emerge. The top-left block $\Lambda_3 = D\Lambda_2 + \Gamma\Gamma^T \Lambda_1$ is clearly still diagonal, since it is a linear combination of products of the diagonal matrices D and $\Gamma\Gamma^T$. Similarly, $\Lambda_2 \Gamma$ must have the same structure as Γ , since it is the product of a diagonal matrix and Γ , and the bottom-left block is still the transpose of the top-right one. Last, the structure of the bottom-right block also remains unchanged, since $D\Gamma$ has the same structure as Γ . Specifically, it must be that $\Gamma^T D \Gamma$ has the same structure as $\Gamma^T \Gamma$, but with $g_{ip_m} g_{ip_n} \rightarrow \Delta_i g_{ip_m} g_{ip_n}$.

In fact, as can be shown via induction, we can write H^k for any $k \geq 1$ as

$$H^k = \begin{bmatrix} \Lambda_k & \Lambda_{k-1} \Gamma \\ \Gamma^T \Lambda_{k-1} & \Gamma^T \Lambda_{k-2} \Gamma \end{bmatrix}, \quad (\text{B12})$$

where $\{\Lambda_k\}_{k=-1}^{\infty}$ is the sequence of diagonal matrices defined by the recursive formula

$$\Lambda_{k+1} = D\Lambda_k + \Gamma\Gamma^T \Lambda_{k-1} \quad (\text{B13})$$

and the seed values

$$\Lambda_{-1} = \mathbb{0}, \quad \Lambda_0 = \mathbb{1}, \quad (\text{B14})$$

where $\mathbb{0}$ and $\mathbb{1}$ are the $M \times M$ zero and identity matrices, respectively.

Thus, defining the diagonal matrices $D_{0,1,2}$ via

$$D_l = \sum_{k \geq 1} \frac{(-i\Delta t)^k}{k!} \Lambda_{k-l}, \quad (\text{B15})$$

we find that

$$\begin{aligned} U_A(\Delta t) &= \mathbb{1} + \begin{bmatrix} D_0 & D_1 \Gamma \\ \Gamma^T D_1 & \Gamma^T D_2 \Gamma \end{bmatrix} \\ &= \begin{bmatrix} \mathbb{1}_M + D_0 & D_1 \Gamma \\ \Gamma^T D_1 & \mathbb{1}_{N^2} + \Gamma^T D_2 \Gamma \end{bmatrix}, \end{aligned} \quad (\text{B16})$$

which is where Eq. (19) comes from.

To derive Eq. (20) from this, we need to examine the elements of the D_l matrices. Since both D_l and Λ_k are diagonal, let us introduce the notation $d_{l,i} = [D_l]_{ii}$ and $\lambda_{k,i} = [\Lambda_k]_{ii}$ (no

sum) for the i th element along their main diagonal, so that

$$d_{l,i} = \sum_{k \geq 1} \frac{(-i\Delta t)^k}{k!} \lambda_{k-l,i}, \quad (\text{B17})$$

where $\{\lambda_{k,i}\}_{k=-1}^{\infty}$ satisfies the recursive formula

$$\lambda_{k+1,i} = \Delta_i \lambda_{k,i} + G_i^2 \lambda_{k-1,i}, \quad (\text{B18})$$

with the seed values $\lambda_{0,i} = 1$ and $\lambda_{-1,i} = 0$.

Defining the effective Hamiltonian

$$H_i = \begin{bmatrix} \Delta_i & G_i \\ G_i & 0 \end{bmatrix}, \quad (\text{B19})$$

we see that its associated evolution operator $U_i(\Delta t) = \exp(-iH_i \Delta t)$ must be equal to

$$\begin{aligned} U_i(\Delta t) &= \mathbb{1} + \begin{bmatrix} d_{0,i} & G_i d_{1,i} \\ G_i d_{1,i} & G_i^2 d_{2,i} \end{bmatrix} \\ &= \begin{bmatrix} 1 + d_{0,i} & G_i d_{1,i} \\ G_i d_{1,i} & 1 + G_i^2 d_{2,i} \end{bmatrix}. \end{aligned} \quad (\text{B20})$$

This follows from the fact that H_i can be seen as a special case of H with $M, N = 1$, $D = [\Delta_i]$ and $\Gamma = [G_i]$.

Comparing this to the elements of U_A , i.e.,

$$\begin{cases} [\mathbb{1}_M + D_0]_{ij} = (1 + d_{0,i})\delta_{ij}, \\ [D_1 \Gamma]_{in} = [\Gamma^T D_1]_{ni} = \begin{cases} g_{ip_n} d_{1,i} & \text{if cavity } n \text{ couples to atom } i \text{ at point } p_n, \\ 0 & \text{otherwise,} \end{cases} \\ [\mathbb{1}_{N^2} + \Gamma^T D_2 \Gamma]_{mn} = \begin{cases} \delta_{mn} + g_{ip_m} g_{ip_n} d_{2,i} & \text{if cavities } m, n \text{ couple to atom } i \text{ at } p_m, p_n, \\ \delta_{mn} & \text{otherwise,} \end{cases} \end{cases} \quad (\text{B21})$$

we finally arrive at equation Eq. (20):

$$\begin{cases} [\mathbb{1}_M + D_0]_{ij} = \delta_{ij} [U_i]_{11}, \\ [D_1 \Gamma]_{in} = [\Gamma^T D_1]_{ni} = \begin{cases} \frac{g_{ip_n}}{G_i} [U_i]_{12} & \text{if cavity } n \text{ couples to atom } i \text{ at point } p_n, \\ 0 & \text{otherwise,} \end{cases} \\ [\mathbb{1}_{N^2} + \Gamma^T D_2 \Gamma]_{mn} = \begin{cases} \delta_{mn} + \frac{g_{ip_m} g_{ip_n}}{G_i^2} ([U_i]_{22} - 1) & \text{if cavities } m, n \text{ couple to atom } i \text{ at } p_m, p_n, \\ \delta_{mn} & \text{otherwise.} \end{cases} \end{cases} \quad (\text{B22})$$

It is possible to save a bit more computation time by pre-computing U_i analytically. Diagonalizing the H_i matrix, we find that its eigenvalues are

$$\kappa_{\pm,i} = \frac{\Delta_i}{2} \pm \sqrt{\frac{\Delta_i^2}{4} + G_i^2}. \quad (\text{B23})$$

By examining the expression for $[H_i^k]_{11} = \lambda_{k,i}$ obtained from diagonalization one can then show that

$$\lambda_{k,i} = \frac{\kappa_{+,i}^{k+1} - \kappa_{-,i}^{k+1}}{\kappa_{+,i} - \kappa_{-,i}}. \quad (\text{B24})$$

This in turn gives us an analytic expression for the elements of D_l , namely,

$$\begin{aligned} d_{l,i} &= \frac{1}{\kappa_+ - \kappa_-} \sum_{k=1}^{\infty} \frac{(-i\Delta t)^k}{k!} (\kappa_+^{k-l+1} - \kappa_-^{k-l+1}) \\ &= \frac{\kappa_+^{1-l} (e^{-i\Delta t \kappa_+} - 1) - \kappa_-^{1-l} (e^{-i\Delta t \kappa_-} - 1)}{\kappa_+ - \kappa_-}, \end{aligned} \quad (\text{B25})$$

where we have suppressed the i index on $\kappa_{\pm,i}$. Inserting these findings into our expressions for the elements of U_i then

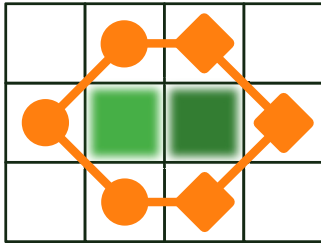


FIG. 14. Perfectly subradiant giant atom with six coupling points (orange marks linked by a solid line) detuned by $\Delta/J = \pm 1$ from the middle of the band. The circles indicate points with coupling strength g_1 , while the squares indicate points with strength g_2 . The green lattice sites show the photonic excitation of the bound state in the continuum, with the intensity of the color referring to the amplitude β_1 (light green) and β_2 (dark green).

gives us

$$\begin{aligned} [U_i]_{11} &= \frac{\kappa_+ e^{-i\Delta t \kappa_+} - \kappa_- e^{-i\Delta t \kappa_-}}{\kappa_+ - \kappa_-}, \\ [U_i]_{12} &= [U_i]_{21} = G_i \frac{e^{-i\Delta t \kappa_+} - e^{-i\Delta t \kappa_-}}{\kappa_+ - \kappa_-}, \\ [U_i]_{22} &= \frac{\kappa_+ e^{-i\Delta t \kappa_-} - \kappa_- e^{-i\Delta t \kappa_+}}{\kappa_+ - \kappa_-}. \end{aligned} \quad (\text{B26})$$

It should be noted that while it is slightly faster to calculate $d_{l,i}$ and U_i by inserting all the relevant quantities into these expressions rather than by numerically computing the 2×2 matrix exponential $\exp(-iH_i \Delta t)$ [at least with SciPy's `linalg.expm()`], the effect of doing so on the speed of the overall time-evolution algorithm is negligible. This is because, as discussed in Sec. III, the FFT and iFFT performed every time step are where the overwhelming majority of the computational cost of the algorithm comes from. However, calculating the elements of U_i using Eq. (B26) tends to give slightly better unitarity than that achieved by naively exponentiating $-iH_i \Delta t$ using SciPy's `linalg.expm()`.

APPENDIX C: PERFECTLY SUBRADIANT CONFIGURATIONS WITH $\Delta/J \neq 0$

In Sec. IV, we focused on configurations of GAs with $\Delta/J = 0$ because they are the simplest to conceive. However, one can also engineer perfect subradiance where the atoms are tuned away from the middle of the band, i.e., with $\Delta/J \neq 0$. In such configurations, the emission to the bath is no longer restricted to the main diagonals and it is thus necessary to completely surround the photonic BIC peaks with coupling points to prevent leakage.

To see this, let us consider a simple example, namely a configuration like the one shown in Fig. 14.

Placing the origin of our coordinate system at the leftmost photonic BIC peak in Fig. 14 and defining

$$\begin{aligned} |B_1\rangle &= \begin{bmatrix} 0 \\ 0 \end{bmatrix}, \\ |B_2\rangle &= \begin{bmatrix} 1 \\ 0 \end{bmatrix}, \end{aligned}$$

$$\begin{aligned} |C_1\rangle &= \left(\begin{bmatrix} -1 \\ 0 \end{bmatrix} + \begin{bmatrix} 0 \\ -1 \end{bmatrix} + \begin{bmatrix} 0 \\ 1 \end{bmatrix} \right) / \sqrt{3}, \\ |C_2\rangle &= \left(\begin{bmatrix} 2 \\ 0 \end{bmatrix} + \begin{bmatrix} 1 \\ -1 \end{bmatrix} + \begin{bmatrix} 1 \\ 1 \end{bmatrix} \right) / \sqrt{3}, \end{aligned} \quad (\text{C1})$$

we can find the dressed excited state $|e'\rangle$ like we did in Sec. IV A 2 by making an ansatz:

$$|e'\rangle = \alpha|e\rangle + \beta_1|B_1\rangle + \beta_2|B_2\rangle. \quad (\text{C2})$$

Applying the Hamiltonian to the state yields

$$\begin{aligned} H|e'\rangle &= \alpha H|e\rangle + \beta_1 H|B_1\rangle + \beta_2 H|B_2\rangle \\ &= \alpha \Delta|e\rangle - \beta_2 J|B_1\rangle - \beta_1 J|B_2\rangle \\ &\quad + (\alpha g_1 - \beta_1 J)\sqrt{3}|C_1\rangle + (\alpha g_2 - \beta_2 J)\sqrt{3}|C_2\rangle. \end{aligned} \quad (\text{C3})$$

Now, demanding $|e'\rangle$ to be an eigenstate, i.e., $H|e'\rangle \propto |e'\rangle$, means that the prefactors of $|C_1\rangle$ and $|C_2\rangle$ need to cancel, which leads to

$$\begin{cases} \beta_1 = \frac{g_1}{J}\alpha \\ \beta_2 = \frac{g_2}{J}\alpha \end{cases} \Rightarrow \frac{\beta_2}{\beta_1} = \frac{g_2}{g_1}. \quad (\text{C4})$$

Note that neither β_1 nor β_2 can be zero if g_1 and g_2 are both nonzero. The condition $H|e'\rangle \propto |e'\rangle$ also implies that the prefactors of $|e\rangle$, $|B_1\rangle$, and $|B_2\rangle$ are scaled by the same factor when H is applied, meaning

$$\begin{cases} \beta_1 = -\frac{\beta_2 J}{\Delta} \\ \beta_2 = -\frac{\beta_1 J}{\Delta} \end{cases} \Rightarrow \frac{\Delta}{J} = -\frac{\beta_2}{\beta_1} = \frac{\beta_1}{\beta_2} = \pm 1, \quad (\text{C5})$$

which is achieved for $g_2/g_1 = \mp 1$.

An interesting consequence of the existence of these kinds of configurations is the fact that it opens up for the possibility of a configuration exhibiting perfect subradiance at several different detunings Δ/J , but with different BIC-peak interference patterns at each detuning. This has only previously been demonstrated in 1D waveguides [5], where it is easier to accomplish thanks to the lack of additional dimensions for the photonic excitation to leak away into. Such a GA can have its interaction through certain BIC peaks turned on and off at will solely by changing the atom's detuning. It should be noted, however, that toggling the interaction in this way would entail a risk of decoherence, since part of the BIC population would be able to escape as the interference pattern reestablishes itself—at least if done naively.

The simplest example of such a configuration is shown in Fig. 15. For this configuration, any choice of detuning $\Delta/J \in \{0, \pm 3\}$ yields perfect subradiance for $g_2 = 3g_1$. The BIC peak amplitudes β_i for the various different choices of detuning can be expressed in terms of $\beta = \alpha g_1/J$ as

$$\begin{cases} \beta_1 = \beta, \\ \beta_2 = 2\beta, \\ \beta_3 = -\frac{\Delta}{J}\beta, \\ \beta_4 = \left(\frac{\Delta^2}{J^2} - 5\right)\beta. \end{cases} \quad (\text{C6})$$

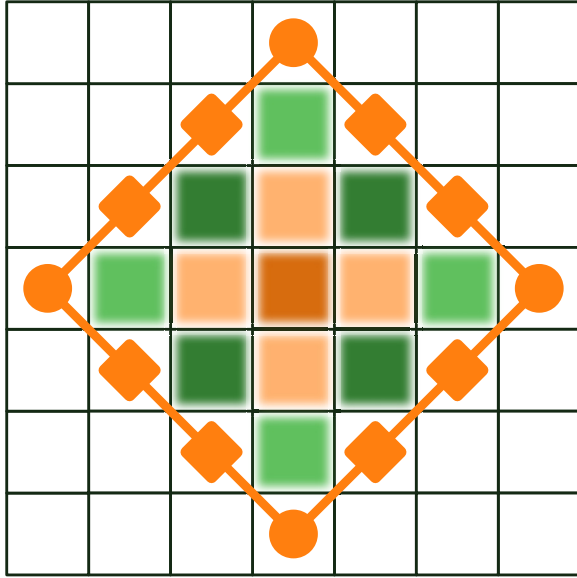


FIG. 15. Perfectly subradiant giant atom with twelve coupling points (orange marks linked by a solid line) detuned by $\Delta/J = \{0, \pm 3\}$ from the middle of the band. The circles indicate points with coupling strength g_1 , while the squares indicate points with strength $g_2 = 3g_1$. The green and orange lattice sites show the photonic excitation of the bound state in the continuum, with the color referring to the amplitude β_1 (light green), β_2 (dark green), β_3 (light orange), and β_4 (dark orange). The green lattice sites are detuning-invariant, the light orange sites are only populated for $\Delta/J = \pm 3$, and the dark orange site has different amplitudes at $\Delta/J = 0$ and ± 3 .

In other words, the peaks labeled 1 and 2 are detuning-invariant, the peaks labeled 3 are only populated for $\Delta/J = \pm 3$ (in which case they have amplitude $\mp 3\beta$), and peak 4 has amplitude -5β (4β) at $\Delta/J = 0$ ($\Delta/J = \pm 3$).

Since even this simplest configuration is quite large, one needs to choose quite a small g_1 to limit the risk of decoherence when toggling the detuning. More specifically, the choices $\Delta/J = 0$ and $\Delta/J = \pm 3$ correspond to

dressed states

$$|e', \Delta/J = 0\rangle = \left[|e\rangle + \frac{g_1}{J}(\sqrt{4}|B_1\rangle + 2\sqrt{4}|B_2\rangle - 5|B_4\rangle) \right] \times \frac{1}{\sqrt{1 + 45g_1^2/J^2}} \quad (\text{C7})$$

and

$$|e', \Delta/J = \pm 3\rangle = \left[|e\rangle + \frac{g_1}{J}(\sqrt{4}|B_1\rangle + 2\sqrt{4}|B_2\rangle \mp 3\sqrt{4}|B_3\rangle + 4|B_4\rangle) \right] \times \frac{1}{\sqrt{1 + 72g_1^2/J^2}}, \quad (\text{C8})$$

respectively. Thus, the probability of decoherence when switching the photonic BIC peaks labeled 3 on or off is approximately

$$p = 1 - |\langle e', \Delta/J = 0 | e', \Delta/J = \pm 3 \rangle|^2 = 1 - \frac{1}{(1 + 45g_1^2/J^2)(1 + 72g_1^2/J^2)} \stackrel{g_1/J \ll 1}{\approx} \approx 117g_1^2/J^2. \quad (\text{C9})$$

Similarly, the probability of decoherence when switching directly between $\Delta/J = +3$ and $\Delta/J = -3$ is approximately

$$p' = 1 - |\langle e', \Delta/J = \pm 3 | e', \Delta/J = \mp 3 \rangle|^2 = 1 - \frac{1}{(1 + 72g_1^2/J^2)^2} \stackrel{g_1/J \ll 1}{\approx} \approx 144g_1^2/J^2. \quad (\text{C10})$$

These values are perhaps even larger than one might naively guess, since the overlaps between the photonic BIC interference patterns corresponding to different choices for $|\Delta/J|$ are zero—all of the overlap between any pair of two different permitted dressed states comes from the overlap between the atomic parts.

-
- [1] A. Frisk Kockum, Quantum optics with giant atoms—The first five years, in *Proceedings of the International Symposium on Mathematics, Quantum Theory, and Cryptography*, edited by T. Takagi, M. Wakayama, K. Tanaka, N. Kunihiro, K. Kimoto, and Y. Ikematsu (Springer, Singapore, 2021), pp. 125–146.
- [2] A. Frisk Kockum, P. Delsing, and G. Johansson, Designing frequency-dependent relaxation rates and Lamb shifts for a giant artificial atom, *Phys. Rev. A* **90**, 013837 (2014).
- [3] A. M. Vadiraj, A. Ask, T. G. McConkey, I. Nsanzineza, C. W. Sandbo Chang, A. F. Kockum, and C. M. Wilson, Engineering the level structure of a giant artificial atom in waveguide quantum electrodynamics, *Phys. Rev. A* **103**, 023710 (2021).
- [4] A. F. Kockum, G. Johansson, and F. Nori, Decoherence-free interaction between giant atoms in waveguide quantum electrodynamics, *Phys. Rev. Lett.* **120**, 140404 (2018).
- [5] B. Kannan, M. J. Ruckriegel, D. L. Campbell, A. Frisk Kockum, J. Braumüller, D. K. Kim, M. Kjaergaard, P. Krantz, A. Melville, B. M. Niedzielski, A. Vepsäläinen, R. Winik, J. L. Yoder, F. Nori, T. P. Orlando, S. Gustavsson, and W. D. Oliver, Waveguide quantum electrodynamics with superconducting artificial giant atoms, *Nature (London)* **583**, 775 (2020).
- [6] A. Carollo, D. Cilluffo, and F. Ciccarello, Mechanism of decoherence-free coupling between giant atoms, *Phys. Rev. Res.* **2**, 043184 (2020).
- [7] A. Soro and A. F. Kockum, Chiral quantum optics with giant atoms, *Phys. Rev. A* **105**, 023712 (2022).
- [8] A. Soro, C. S. Muñoz, and A. F. Kockum, Interaction between giant atoms in a one-dimensional structured environment, *Phys. Rev. A* **107**, 013710 (2023).
- [9] L. Du, L. Guo, and Y. Li, Complex decoherence-free interactions between giant atoms, *Phys. Rev. A* **107**, 023705 (2023).

- [10] L. Guo, A. F. Kockum, F. Marquardt, and G. Johansson, Oscillating bound states for a giant atom, *Phys. Rev. Res.* **2**, 043014 (2020).
- [11] S. Guo, Y. Wang, T. Purdy, and J. Taylor, Beyond spontaneous emission: Giant atom bounded in the continuum, *Phys. Rev. A* **102**, 033706 (2020).
- [12] S. Terradas-Briansó, C. A. González-Gutiérrez, F. Nori, L. Martín-Moreno, and D. Zueco, Ultrastrong waveguide QED with giant atoms, *Phys. Rev. A* **106**, 063717 (2022).
- [13] D. D. Noachtar, J. Knörzer, and R. H. Jonsson, Nonperturbative treatment of giant atoms using chain transformations, *Phys. Rev. A* **106**, 013702 (2022).
- [14] K. H. Lim, W. K. Mok, and L. C. Kwek, Oscillating bound states in non-Markovian photonic lattices, *Phys. Rev. A* **107**, 023716 (2023).
- [15] M. V. Gustafsson, T. Aref, A. F. Kockum, M. K. Ekström, G. Johansson, and P. Delsing, Propagating phonons coupled to an artificial atom, *Science* **346**, 207 (2014).
- [16] T. Aref, P. Delsing, M. K. Ekström, A. F. Kockum, M. V. Gustafsson, G. Johansson, P. J. Leek, E. Magnusson, and R. Manenti, Quantum acoustics with surface acoustic waves, in *Superconducting Devices in Quantum Optics*, edited by R. H. Hadfield and G. Johansson (Springer, Berlin, 2016).
- [17] R. Manenti, A. F. Kockum, A. Patterson, T. Behrle, J. Rahamim, G. Tancredi, F. Nori, and P. J. Leek, Circuit quantum acoustodynamics with surface acoustic waves, *Nat. Commun.* **8**, 975 (2017).
- [18] A. Noguchi, R. Yamazaki, Y. Tabuchi, and Y. Nakamura, Qubit-assisted transduction for a detection of surface acoustic waves near the quantum limit, *Phys. Rev. Lett.* **119**, 180505 (2017).
- [19] K. J. Satzinger, Y. P. Zhong, H.-S. Chang, G. A. Peairs, A. Bienfait, M.-H. Chou, A. Y. Cleland, C. R. Conner, É. Dumur, J. Grebel, I. Gutierrez, B. H. November, R. G. Povey, S. J. Whiteley, D. D. Awschalom, D. I. Schuster, and A. N. Cleland, Quantum control of surface acoustic-wave phonons, *Nature (London)* **563**, 661 (2018).
- [20] B. A. Moores, L. R. Sletten, J. J. Viennot, and K. W. Lehnert, Cavity quantum acoustic device in the multimode strong coupling regime, *Phys. Rev. Lett.* **120**, 227701 (2018).
- [21] A. N. Bolgar, J. I. Zotova, D. D. Kirichenko, I. S. Besedin, A. V. Semenov, R. S. Shaikhaidarov, and O. V. Astafiev, Quantum regime of a two-dimensional phonon cavity, *Phys. Rev. Lett.* **120**, 223603 (2018).
- [22] L. R. Sletten, B. A. Moores, J. J. Viennot, and K. W. Lehnert, Resolving phonon fock states in a multimode cavity with a double-slit qubit, *Phys. Rev. X* **9**, 021056 (2019).
- [23] A. Bienfait, K. J. Satzinger, Y. P. Zhong, H.-S. Chang, M.-H. Chou, C. R. Conner, É. Dumur, J. Grebel, G. A. Peairs, R. G. Povey, and A. N. Cleland, Phonon-mediated quantum state transfer and remote qubit entanglement, *Science* **364**, 368 (2019).
- [24] G. Andersson, B. Suri, L. Guo, T. Aref, and P. Delsing, Non-exponential decay of a giant artificial atom, *Nat. Phys.* **15**, 1123 (2019).
- [25] A. Bienfait, Y. P. Zhong, H.-S. Chang, M.-H. Chou, C. R. Conner, É. Dumur, J. Grebel, G. A. Peairs, R. G. Povey, K. J. Satzinger, and A. N. Cleland, Quantum erasure using entangled surface acoustic phonons, *Phys. Rev. X* **10**, 021055 (2020).
- [26] G. Andersson, M. K. Ekström, and P. Delsing, Electromagnetically induced acoustic transparency with a superconducting circuit, *Phys. Rev. Lett.* **124**, 240402 (2020).
- [27] C. Joshi, F. Yang, and M. Mirhosseini, Resonance fluorescence of a chiral artificial atom, *Phys. Rev. X* **13**, 021039 (2023).
- [28] A. González-Tudela, C. S. Muñoz, and J. I. Cirac, Engineering and harnessing giant atoms in high-dimensional baths: A proposal for implementation with cold atoms, *Phys. Rev. Lett.* **122**, 203603 (2019).
- [29] L. Du, Y. Zhang, J. H. Wu, A. F. Kockum, and Y. Li, Giant atoms in a synthetic frequency dimension, *Phys. Rev. Lett.* **128**, 223602 (2022).
- [30] P. O. Guimond, B. Vermersch, M. L. Juan, A. Sharafiev, G. Kirchmair, and P. Zoller, A unidirectional on-chip photonic interface for superconducting circuits, *npj Quantum Inf.* **6**, 32 (2020).
- [31] N. Gheeraert, S. Kono, and Y. Nakamura, Programmable directional emitter and receiver of itinerant microwave photons in a waveguide, *Phys. Rev. A* **102**, 053720 (2020).
- [32] Y. X. Zhang, C. R. Carceller, M. Kjaergaard, and A. S. Sørensen, Charge-noise insensitive chiral photonic interface for waveguide circuit QED, *Phys. Rev. Lett.* **127**, 233601 (2021).
- [33] X.-L. Yin, Y.-H. Liu, J.-F. Huang, and J.-Q. Liao, Single-photon scattering in a giant-molecule waveguide-QED system, *Phys. Rev. A* **106**, 013715 (2022).
- [34] B. Kannan, A. Almanakly, Y. Sung, A. Di Paolo, D. A. Rower, J. Braumüller, A. Melville, B. M. Niedzielski, A. Karamlou, K. Serniak, A. Vepsäläinen, M. E. Schwartz, J. L. Yoder, R. Winik, J. I. Wang, T. P. Orlando, S. Gustavsson, J. A. Grover, and W. D. Oliver, On-demand directional microwave photon emission using waveguide quantum electrodynamics, *Nat. Phys.* **19**, 394 (2023).
- [35] Z. Q. Wang, Y. P. Wang, J. Yao, R. C. Shen, W. J. Wu, J. Qian, J. Li, S. Y. Zhu, and J. Q. You, Giant spin ensembles in waveguide magnonics, *Nat. Commun.* **13**, 7580 (2022).
- [36] L. Guo, A. L. Grimsmo, A. F. Kockum, M. Pletyukhov, and G. Johansson, Giant acoustic atom: A single quantum system with a deterministic time delay, *Phys. Rev. A* **95**, 053821 (2017).
- [37] T. M. Karg, B. Gouraud, P. Treutlein, and K. Hammerer, Remote Hamiltonian interactions mediated by light, *Phys. Rev. A* **99**, 063829 (2019).
- [38] A. Ask, Y.-L. L. Fang, and A. F. Kockum, Synthesizing electromagnetically induced transparency without a control field in waveguide QED using small and giant atoms, [arXiv:2011.15077](https://arxiv.org/abs/2011.15077).
- [39] L. Du and Y. Li, Single-photon frequency conversion via a giant Λ -type atom, *Phys. Rev. A* **104**, 023712 (2021).
- [40] S. L. Feng and W. Z. Jia, Manipulating single-photon transport in a waveguide-QED structure containing two giant atoms, *Phys. Rev. A* **104**, 063712 (2021).
- [41] Q. Y. Cai and W. Z. Jia, Coherent single-photon scattering spectra for a giant-atom waveguide-QED system beyond the dipole approximation, *Phys. Rev. A* **104**, 033710 (2021).
- [42] X.-L. Yin, W.-B. Luo, and J.-Q. Liao, Non-Markovian disentanglement dynamics in double-giant-atom waveguide-QED systems, *Phys. Rev. A* **106**, 063703 (2022).

- [43] Y.-T. Chen, L. Du, L. Guo, Z. Wang, Y. Zhang, Y. Li, and J.-H. Wu, Nonreciprocal and chiral single-photon scattering for giant atoms, *Commun. Phys.* **5**, 215 (2022).
- [44] L. Du, Y.-T. Chen, Y. Zhang, and Y. Li, Giant atoms with time-dependent couplings, *Phys. Rev. Res.* **4**, 023198 (2022).
- [45] L. Du, Y. Zhang, and Y. Li, A giant atom with modulated transition frequency, *Front. Phys.* **18**, 12301 (2023).
- [46] A. C. Santos and R. Bachelard, Generation of maximally entangled long-lived states with giant atoms in a waveguide, *Phys. Rev. Lett.* **130**, 053601 (2023).
- [47] X. Wang, H.-B. Zhu, T. Liu, and F. Nori, Realizing quantum optics in structured environments with giant atoms, *Phys. Rev. Res.* **6**, 013279 (2024).
- [48] J. Zhou, X.-L. Yin, and J.-Q. Liao, Chiral and nonreciprocal single-photon scattering in a chiral-giant-molecule waveguide-QED system, *Phys. Rev. A* **107**, 063703 (2023).
- [49] W. Gu, H. Huang, Z. Yi, L. Chen, L. Sun, and H. Tan, Correlated two-photon scattering in a one-dimensional waveguide coupled to two- or three-level giant atoms, *Phys. Rev. A* **108**, 053718 (2023).
- [50] L. Xu and L. Guo, Catch and release of propagating bosonic field with non-Markovian giant atom, *New J. Phys.* **26**, 013025 (2024).
- [51] S. Longhi, Photonic simulation of giant atom decay, *Opt. Lett.* **45**, 3017 (2020).
- [52] W. Zhao and Z. Wang, Single-photon scattering and bound states in an atom-waveguide system with two or multiple coupling points, *Phys. Rev. A* **101**, 053855 (2020).
- [53] X. Wang, T. Liu, A. F. Kockum, H.-R. Li, and F. Nori, Tunable chiral bound states with giant atoms, *Phys. Rev. Lett.* **126**, 043602 (2021).
- [54] S. Longhi, Rabi oscillations of bound states in the continuum, *Opt. Lett.* **46**, 2091 (2021).
- [55] H. Yu, Z. Wang, and J.-H. Wu, Entanglement preparation and nonreciprocal excitation evolution in giant atoms by controllable dissipation and coupling, *Phys. Rev. A* **104**, 013720 (2021).
- [56] C. Vega, M. Bello, D. Porras, and A. González-Tudela, Qubit-photon bound states in topological waveguides with long-range hoppings, *Phys. Rev. A* **104**, 053522 (2021).
- [57] X. Wang and H.-r. Li, Chiral quantum network with giant atoms, *Quantum Sci. Technol.* **7**, 035007 (2022).
- [58] H. Xiao, L. Wang, Z. Li, X. Chen, and L. Yuan, Bound state in a giant atom-modulated resonators system, *npj Quantum Inf.* **8**, 80 (2022).
- [59] W. Cheng, Z. Wang, and Y. X. Liu, Topology and retardation effect of a giant atom in a topological waveguide, *Phys. Rev. A* **106**, 033522 (2022).
- [60] X. Zhang, W. Cheng, Z. Gong, T. Zheng, and Z. Wang, Superconducting giant atom waveguide QED: Quantum Zeno and anti-Zeno effects in ultrastrong coupling regime, [arXiv:2205.03674](https://arxiv.org/abs/2205.03674).
- [61] L. Du, L. Guo, Y. Zhang, and A. F. Kockum, Giant emitters in a structured bath with non-Hermitian skin effect, *Phys. Rev. Res.* **5**, L042040 (2023).
- [62] L. Du, Y.-T. Chen, Y. Zhang, Y. Li, and J.-H. Wu, Decay dynamics of a giant atom in a structured bath with broken time-reversal symmetry, *Quantum Sci. Technol.* **8**, 045010 (2023).
- [63] R. Bag and D. Roy, Quantum light-matter interactions in structured waveguides, *Phys. Rev. A* **108**, 053717 (2023).
- [64] W. Z. Jia and M. T. Yu, Atom-photon dressed states in a waveguide-QED system with multiple giant atoms, *Opt. Express* **32**, 9495 (2024).
- [65] Z.-M. Gao, J.-Q. Li, Z.-W. Li, W.-X. Liu, and X. Wang, Circuit QED with giant atoms coupling to left-handed superlattice metamaterials, *Phys. Rev. A* **109**, 013716 (2024).
- [66] A. González-Tudela and J. I. Cirac, Markovian and non-Markovian dynamics of quantum emitters coupled to two-dimensional structured reservoirs, *Phys. Rev. A* **96**, 043811 (2017).
- [67] A. González-Tudela and J. I. Cirac, Quantum emitters in two-dimensional structured reservoirs in the nonperturbative regime, *Phys. Rev. Lett.* **119**, 143602 (2017).
- [68] F. Galve and R. Zambrini, Completely subradiant multi atom architectures through 2D photonic crystals, *Annalen der Physik* **530**, 1800017 (2018).
- [69] S.-P. Yu, J. A. Muniz, C.-L. Hung, and H. J. Kimble, Two-dimensional photonic crystals for engineering atom light interactions, *Proc. Natl. Acad. Sci. USA* **116**, 12743 (2019).
- [70] A. Feiguin, J. J. García-Ripoll, and A. González-Tudela, Qubit-photon corner states in all dimensions, *Phys. Rev. Res.* **2**, 023082 (2020).
- [71] L. Ruks and T. Busch, Green's functions of and emission into discrete anisotropic and hyperbolic baths, *Phys. Rev. Res.* **4**, 023044 (2022).
- [72] C. Vega, D. Porras, and A. González-Tudela, Topological multimode waveguide QED, *Phys. Rev. Res.* **5**, 023031 (2023).
- [73] B. Windt, M. Bello, E. Demler, and J. I. Cirac, Fermionic matter-wave quantum optics with cold-atom impurity models, *Phys. Rev. A* **109**, 023306 (2024).
- [74] A. González-Tudela and J. I. Cirac, Exotic quantum dynamics and purely long-range coherent interactions in Dirac conelike baths, *Phys. Rev. A* **97**, 043831 (2018).
- [75] P. Bienias, I. Boettcher, R. Belyansky, A. J. Kollár, and A. V. Gorshkov, Circuit quantum electrodynamics in hyperbolic space: From photon bound states to frustrated spin models, *Phys. Rev. Lett.* **128**, 013601 (2022).
- [76] D. De Bernardis, F. S. Piccioli, P. Rabl, and I. Carusotto, Chiral quantum optics in the bulk of photonic quantum Hall systems, *PRX Quantum* **4**, 030306 (2023).
- [77] M. Tečer, M. Di Liberto, P. Silvi, S. Montangero, F. Romanato, and G. Calajó, Strongly Interacting Photons in 2D Waveguide QED, *Phys. Rev. Lett.* **132**, 163602 (2024).
- [78] A. González-Tudela and J. I. Cirac, Non-Markovian quantum optics with three-dimensional state-dependent optical lattices, *Quantum* **2**, 97 (2018).
- [79] I. García-Elcano, A. González-Tudela, and J. Bravo-Abad, Tunable and robust long-range coherent interactions between quantum emitters mediated by Weyl bound states, *Phys. Rev. Lett.* **125**, 163602 (2020).
- [80] I. García-Elcano, J. Merino, J. Bravo-Abad, and A. González-Tudela, Probing and harnessing photonic Fermi arc surface states using light-matter interactions, *Sci. Adv.* **9**, eadf8257 (2023).
- [81] L. Leonforte, X. Sun, D. Valenti, B. Spagnolo, F. Illuminati, A. Carollo, and F. Ciccarello, Quantum optics with giant atoms in a structured photonic bath, [arXiv:2402.10275](https://arxiv.org/abs/2402.10275).

- [82] J. von Neumann and E. Wigner, Über merkwürdige diskrete Eigenwerte. Über das Verhalten von Eigenwerten bei adiabatischen Prozessen, *Physica Z* **30**, 467 (1929).
- [83] C. W. Hsu, B. Zhen, A. D. Stone, J. D. Joannopoulos, and M. Soljačić, Bound states in the continuum, *Nat. Rev. Mater.* **1**, 16048 (2016).
- [84] M. Kang, T. Liu, C. T. Chan, and M. Xiao, Applications of bound states in the continuum in photonics, *Nat. Rev. Phys.* **5**, 659 (2023).
- [85] G. Xu, H. Xing, Z. Xue, D. Lu, J. Fan, J. Fan, P. P. Shum, and L. Cong, Recent advances and perspective of photonic bound states in the continuum, *Ultrafast Sci.* **3**, 0033 (2023).
- [86] Code available at <https://github.com/ariadna-soro/Ingelsten2024>.
- [87] P. Roushan, C. Neill, A. Megrant, Y. Chen, R. Babbush, R. Barends, B. Campbell, Z. Chen, B. Chiaro, A. Dunsworth, A. Fowler, E. Jeffrey, J. Kelly, E. Lucero, J. Mutus, P. J. J. O'Malley, M. Neeley, C. Quintana, D. Sank, A. Vainsencher *et al.*, Chiral ground-state currents of interacting photons in a synthetic magnetic field, *Nat. Phys.* **13**, 146 (2017).
- [88] P. Lodahl, S. Mahmoodian, S. Stobbe, A. Rauschenbeutel, P. Schneeweiss, J. Volz, H. Pichler, and P. Zoller, Chiral quantum optics, *Nature (London)* **541**, 473 (2017).
- [89] J. D. Hood, A. Goban, A. Asenjo-Garcia, M. Lu, S. P. Yu, D. E. Chang, and H. J. Kimble, Atom-atom interactions around the band edge of a photonic crystal waveguide, *Proc. Natl. Acad. Sci. USA* **113**, 10507 (2016).
- [90] L. Krinner, M. Stewart, A. Pazmiño, J. Kwon, and D. Schneble, Spontaneous emission of matter waves from a tunable \hat{A} open quantum system, *Nature (London)* **559**, 589 (2018).
- [91] M. Stewart, J. Kwon, A. Lanuza, and D. Schneble, Dynamics of matter-wave quantum emitters in a structured vacuum, *Phys. Rev. Res.* **2**, 043307 (2020).
- [92] Y. Liu and A. A. Houck, Quantum electrodynamics near a photonic bandgap, *Nat. Phys.* **13**, 48 (2017).
- [93] N. M. Sundaresan, R. Lundgren, G. Zhu, A. V. Gorshkov, and A. A. Houck, Interacting qubit-photon bound states with superconducting circuits, *Phys. Rev. X* **9**, 011021 (2019).
- [94] P. M. Harrington, M. Naghiloo, D. Tan, and K. W. Murch, Bath engineering of a fluorescing artificial atom with a photonic crystal, *Phys. Rev. A* **99**, 052126 (2019).
- [95] A. J. Kollár, M. Fitzpatrick, and A. A. Houck, Hyperbolic lattices in circuit quantum electrodynamics, *Nature (London)* **571**, 45 (2019).
- [96] I. Carusotto, A. A. Houck, A. J. Kollár, P. Roushan, D. I. Schuster, and J. Simon, Photonic materials in circuit quantum electrodynamics, *Nat. Phys.* **16**, 268 (2020).
- [97] M. Mirhosseini, E. Kim, V. S. Ferreira, M. Kalaei, A. Sipahigil, A. J. Keller, and O. Painter, Superconducting metamaterials for waveguide quantum electrodynamics, *Nat. Commun.* **9**, 3706 (2018).
- [98] S. Indrajit, H. Wang, M. D. Hutchings, B. G. Taketani, F. K. Wilhelm, M. D. Lahaye, and B. L. T. Plourde, Coupling a superconducting qubit to a left-handed metamaterial resonator, *Phys. Rev. Appl.* **14**, 064033 (2020).
- [99] E. Kim, X. Zhang, V. S. Ferreira, J. Banker, J. K. Iverson, A. Sipahigil, M. Bello, A. González-Tudela, M. Mirhosseini, and O. Painter, Quantum electrodynamics in a topological waveguide, *Phys. Rev. X* **11**, 011015 (2021).
- [100] V. S. Ferreira, J. Banker, A. Sipahigil, M. H. Matheny, A. J. Keller, E. Kim, M. Mirhosseini, and O. Painter, Collapse and revival of an artificial atom coupled to a structured photonic reservoir, *Phys. Rev. X* **11**, 041043 (2021).
- [101] M. Scigliuzzo, G. Calajò, F. Ciccarello, D. Perez Lozano, A. Bengtsson, P. Scarlino, A. Wallraff, D. Chang, P. Delsing, and S. Gasparinetti, Controlling atom-photon bound states in an array of Josephson-junction resonators, *Phys. Rev. X* **12**, 031036 (2022).
- [102] X. Zhang, E. Kim, D. K. Mark, S. Choi, and O. Painter, A superconducting quantum simulator based on a photonic-bandgap metamaterial, *Science* **379**, 278 (2023).
- [103] V. Jouanny, S. Frasca, V. J. Weibel, L. Peyruchat, M. Scigliuzzo, F. Oppliger, F. D. Palma, D. Sbroggio, G. Beaulieu, O. Zilberberg, and P. Scarlino, Band engineering and study of disorder using topology in compact high kinetic inductance cavity arrays, [arXiv:2403.18150](https://arxiv.org/abs/2403.18150).
- [104] D. Rosenberg, D. Kim, R. Das, D. Yost, S. Gustavsson, D. Hover, P. Krantz, A. Melville, L. Racz, G. O. Samach, S. J. Weber, F. Yan, J. L. Yoder, A. J. Kerman, and W. D. Oliver, 3D integrated superconducting qubits, *npj Quantum Inf.* **3**, 42 (2017).
- [105] J. Rahamim, T. Behrle, M. J. Peterer, A. Patterson, P. A. Spring, T. Tsunoda, R. Manenti, G. Tancredi, and P. J. Leek, Double-sided coaxial circuit QED with out-of-plane wiring, *Appl. Phys. Lett.* **110**, 222602 (2017).
- [106] S. Kosen, H.-X. Li, M. Rommel, D. Shiri, C. Warren, L. Grönberg, J. Salonen, T. Abad, J. Biznárová, M. Caputo, L. Chen, K. Grigoras, G. Johansson, A. F. Kockum, C. Križan, D. P. Lozano, G. J. Norris, A. Osman, J. Fernández-Pendás, A. Ronzani *et al.*, Building blocks of a flip-chip integrated superconducting quantum processor, *Quantum Sci. Technol.* **7**, 035018 (2022).
- [107] W. H. Press, S. A. Teukolsky, W. T. Vetterling, and B. P. Flannery, *Numerical Recipes: The Art of Scientific Computing*, 3rd ed. (Cambridge University Press, Cambridge, UK, 2007).
- [108] N. Hatano and M. Suzuki, Finding exponential product formulas of higher orders, in *Quantum Annealing and Other Optimization Methods*, edited by A. Das and B. K. Chakrabarti (Springer, Berlin, 2005), pp. 37–68.
- [109] A. Al-Mohy and N. Higham, A new scaling and squaring algorithm for the matrix exponential, *SIAM J. Matrix Anal. Appl.* **31**, 970 (2010).
- [110] C. Moler and C. Loan, Nineteen dubious ways to compute the exponential of a matrix, twenty-five years later, *Soc. Industr. Appl. Math.* **45**, 3 (2003).
- [111] J. W. Cooley and J. W. Tukey, An algorithm for the machine calculation of complex fourier series, *Math. Comput.* **19**, 297 (1965).
- [112] R. H. Dicke, Coherence in spontaneous radiation processes, *Phys. Rev.* **93**, 99 (1954).
- [113] M. Gross and S. Haroche, Superradiance: An essay on the theory of collective spontaneous emission, *Phys. Rep.* **93**, 301 (1982).
- [114] X. Zhang, C. Liu, Z. Gong, and Z. Wang, Quantum interference and controllable magic cavity QED via a giant atom in

- a coupled resonator waveguide, *Phys. Rev. A* **108**, 013704 (2023).
- [115] L. Du, M.-R. Cai, J.-H. Wu, Z. Wang, and Y. Li, Single-photon nonreciprocal excitation transfer with non-Markovian retarded effects, *Phys. Rev. A* **103**, 053701 (2021).
- [116] G. Calajó, F. Ciccarello, D. Chang, and P. Rabl, Atom-field dressed states in slow-light waveguide QED, *Phys. Rev. A* **93**, 033833 (2016).
- [117] S. Bay, P. Lambropoulos, and K. Mølmer, Atom-atom interaction in strongly modified reservoirs, *Phys. Rev. A* **55**, 1485 (1997).
- [118] P. Lambropoulos, G. M. Nikolopoulos, T. R. Nielsen, and S. Bay, Fundamental quantum optics in structured reservoirs, *Rep. Prog. Phys.* **63**, 455 (2000).
- [119] E. Shahmoon and G. Kurizki, Nonradiative interaction and entanglement between distant atoms, *Phys. Rev. A* **87**, 033831 (2013).
- [120] S. Korenblit, D. Kafri, W. C. Campbell, R. Islam, E. E. Edwards, Z. X. Gong, G. D. Lin, L. M. Duan, J. Kim, K. Kim, and C. Monroe, Quantum simulation of spin models on an arbitrary lattice with trapped ions, *New J. Phys.* **14**, 095024 (2012).
- [121] M. Qiao, Z. Cai, Y. Wang, B. Du, N. Jin, W. Chen, P. Wang, C. Luan, E. Gao, X. Sun, H. Tian, J. Zhang, and K. Kim, Tunable quantum simulation of spin models with a two-dimensional ion crystal, *Nat. Phys.* **20**, 623 (2024).
- [122] B. Fauseweh, Quantum many-body simulations on digital quantum computers: State-of-the-art and future challenges, *Nat. Commun.* **15**, 2123 (2024).
- [123] G. Chen and A. F. Kockum, Simulating open quantum systems with giant atoms, [arXiv:2406.13678](https://arxiv.org/abs/2406.13678).
- [124] C. Cohen-Tannoudji, J. Dupont-Roc, and G. Grynberg, Non-perturbative calculation of transition amplitudes, in *Atom Photon Interactions* (John Wiley & Sons, New York, NY, 1998), Chap. 3, pp. 165–255.
- [125] T. Morita, Useful procedure for computing the lattice Green's function-square, tetragonal, and bcc lattices, *J. Math. Phys.* **12**, 1744 (1971).